Carbon and Carbon/Metal Hybrid Structures Enabled by Ultrafast Heating Methods

Leo Lai, Jing Li, Yeyu Deng, Zixun Yu, Li Wei,* and Yuan Chen*

High-temperature thermal treatment is a standard step in synthesis of many materials. Recently, ultrafast heating methods, such as Joule heating, laser, light, or microwave irradiations, have been used to create novel carbon materials and carbon/metal hybrid structures, demonstrating unique and often superior properties compared with those synthesized by conventional heating methods. They have shown promising application potentials in catalysis, batteries, supercapacitors, fuel cells, sensors, implants, actuators, lighting devices, and waste recycling. Herein, recent findings in creating novel carbon and carbon/metal hybrid structures by ultrafast heating methods are reviewed. The most frequently used ultrafast heating methods, their advantages, and their limitations are first described. Then, different carbon structures created by these methods, including graphene, reduced graphene oxide, hard carbon, carbon nanotube architectures, and other carbon hybrids, are summarized. Next, novel carbon/metal hybrid structures are reviewed, including carbon-supported nanoparticles of monometals, metal alloys, metal composites, high-entropy alloys, and single-atom catalysts. Heating methods, critical precursors used, synthesis parameters affecting material structures, and mechanistic understanding of their unique synthesis processes are focused on. The essential properties of these novel structures and their applications are also summarized. Finally, knowledge gaps and technical challenges in using these methods for scalable material production are discussed.

1. Introduction

Carbon materials are often produced via carbonization, ranging from carbon black, activated carbon, graphene, carbon nanotubes (CNTs), and carbon dots to carbon fibers. Carbonization converts carbon-containing gas, liquid, or solid precursors into solid carbon materials under heat treatment, usually up to 1773 K in inert atmosphere. During carbonization, the heating drives the removal of non-carbon species in the precursors in a sequence following their bonding strength with the carbon matrix. For example, oxygen (O) and nitrogen (N) start to be removed from around 873 K, and hydrogen (H) is removed from

L. Lai, J. Li, Y. Deng, Z. Yu, L. Wei, Y. Chen
School of Chemical and Biomolecular Engineering
The University of Sydney
Darlington, NSW 2006, Australia
E-mail: l.wei@sydney.edu.au; yuan.chen@sydney.edu.au

1273 to 1573 K. Heating carbon sources beyond the carbonization temperature (e.g., 2773 K) results in highly graphitic carbon structures with long-range orders, known as graphitization. Alternatively, small and randomly stacked (turbostratic) carbon layers can grow in different sizes with different graphitic regularities.[1] The traditional heating methods used for carbonization and graphitization include using conventional furnaces, spray pyrolysis, or solvothermal reactors. The thermal energy is transferred from the heating element of a heating instrument to carbon precursors via thermal radiation, convection, or conduction through various mediums. The heating rate is typically below 100 K min^{-1}. Extensive studies have shown that carbon materials' structure and texture strongly depend on their heat treatment temperature, heating/cooling rates, duration, and environment.[1]

Several methods can achieve fast heating of carbon-containing precursors, such as Joule heating, laser irradiation, arc discharging, microwave irradiation, induction heating, or electron beam irradiation, delivering much faster heating rates, for example, $>10^5$ K s^{-1}. Some fast-heating methods played critical roles in the discovery of new carbon nanomaterials. For example, in the soot of laser-irradiated graphite, C_{60} was first discovered.[2] Heating carbon electrodes by arc discharge led to the atomic structure identification of CNTs.[3] In the past few years, several ultrafast heating methods, especially Joule heating, laser, light, and microwave irradiations, have been used to synthesize various carbon structures, including graphene, reduced graphene oxide (rGO), CNT architectures, hard carbon, carbon hybrids, and carbon/metal hybrids. These carbon and carbon/metal structures have been explored in many applications, such as catalysts, batteries, supercapacitors, fuel cells, sensors, implants, actuators, lighting devices, and waste recycling. In this context, this review summarizes recent results (i.e., since 2015) regarding ultrafast heating-enabled carbon materials and carbon/metal hybrid structures. It should be noted that one material often has been explored for multiple applications. We would like to focus on their synthesis methods, critical factors affecting material structures, and current mechanistic understanding of their synthesis processes rather than their specific applications. We first briefly describe several of the most frequently used ultrafast heating methods. Next, we examine carbon structures obtained using

these methods, followed by carbon/metal hybrid structures. The essential properties of these novel structures are also summarized and compared. We only briefly mentioned the key application of each type of material reported in their original publication. In the end, we provide our views on the knowledge gap in understanding ultrafast heating synthesis methods and the critical technical challenges of using these methods for scalable material production.

2. Ultrafast Heating Methods

2.1. Joule Heating

Heat is generated when an electrical current travels through an electrical conductor, known as Joule heating or ohmic (resistive) heating. Joule heating is widely used by metal or graphite heating elements in conventional furnaces. However, few previous studies have used Joule heating to directly heat carbon precursors for carbonization or graphitization. Direct Joule heating of carbon precursors brings several unique advantages. First, the heating and cooling speeds can be several orders faster than conventional heating methods, which enables faster precursor decomposition and avoids the rapid aggregation of metal species at high temperatures. Second, Joule heating can introduce confined high-temperature spots based on the local resistance of carbon precursors, which can be used to achieve targeted heat treatment at a specific location while minimizing the disturbance to the original structure of the precursors. Third, directly heating carbon precursors may significantly reduce the energy consumption associated with carbonization/graphitization. The heat loss to the surrounding medium and undesired heat dissipation could be reduced considerably. With sufficient current density, the flow of electrons can also induce electromigration, which refers to the movement of carbon atoms. This effect, coupled with the extreme temperatures generated by resistive heating, has been proposed to be responsible for the breakdown and rearrangement of the carbon structures during Joule heating.[4] A disadvantage of Joule heating is that it can only work on electrically conductive materials with suitable electrical conductivity, limiting the choice of precursors. Insulating precursors must be mixed with conductive materials so Joule heating can work properly. Joule's law can describe the rate of Joule heating. Assuming the heat generated has all been used to increase the temperature of carbon material, the heating rate can be estimated by the mass and heat capacity of the carbon material.

$$P = IV = I^2 R \tag{1}$$

$$\frac{dT}{dt} = \frac{P}{C_P \rho} \tag{2}$$

where P is the power generated during joule heating (W), I is the electric current (A), V is the electric potential (V), R is the resistance (Ω), C_P is the specific heat capacity (J K^{-1} kg^{-1}), ρ is the density (kg m^{-3}), and dT/dt is the heating rate (K s^{-1}).

Several recent groundbreaking studies have opened new research directions for creating novel carbon materials and carbon/metal hybrids by Joule heating. For example, in 2016,

Yao et al. used Joule heating to weld a carbon nanofiber (CNF) network at temperatures over 2500 K with a heating rate of over 200 K min^{-1}.[5] CNFs were welded together at their junctions due to heating spots created by higher contact resistances at overlapped fiber/fiber junctions (**Figure 1**a). The electrical conductivity of the treated CNF network was improved by order of 4, from the original 0.0133 to 380 S cm^{-1}. Further studies revealed that less conductive amorphous carbon at carbon fiber junctions was key to the carbon welding process.[6] This carbon welding method enabled by Joule heating can be extended to other carbon materials, opening the possibility of creating various carbon structures with improved electrical conductivity. A recent development is a high-throughput roll-to-roll process, which uses Joule heating to convert chemically rGO films into flexible and highly conductive (4200 S cm^{-1}) graphene films (Figure 1b).[7]

Next, in 2018, Yao et al. used Joule heating to synthesize high-entropy-alloy (HEA) nanoparticles on carbon substrates. Carbon materials deposited with different metal precursors were heated by Joule heating over 2000 K with an ultrafast heating rate over 10^5 K s^{-1}.[8] The ultrafast heating rate enabled the rapid decomposition and dispersion of the metal precursors over carbon surfaces, followed by rapid cooling that minimized the high-temperature exposure period to 55 ms. This process efficiently inhibited the aggregation of metal nanoparticles, resulting in the even distribution of metal elements in HEA nanoparticles. Similar approaches have also been used to synthesize carbon/metal hybrids containing various metal species. We will discuss the details of these materials in the later section.

Furthermore, in 2020, Tour's group applied a flash Joule heating method to synthesize turbostratic graphene at a gram scale from a wide range of different carbon precursors.[9] As shown in Figure 1c, solid carbon precursor powders are loosely packed between two Cu electrodes inside a quartz tube, which is different from the standard Joule heating methods performed on carbon materials with more rigid physical structures, such as CNFs and GO films.[9,10] A capacitor bank (with a total capacitance of 0.22 F) was used to deliver the electricity. Carbon precursors were heated above 3000 K in less than 100 ms, causing rapid removal of noncarbon elements and the conversion of amorphous carbon into highly graphitic turbostratic graphene. The output of the capacitor bank can be used to control the peak temperature achieved during Joule heating. This new method suggests a new pathway toward the bulk synthesis of graphene materials. It has also been explored to convert plastic wastes, rubbers, and municipal solid wastes into graphene materials.[11] This method's recent development was synthesizing heteroatom-doped, turbostratic graphene from a wide range of accessible heteroatom sources, including elemental materials, organic compounds, and oxides. Single-element-doped and up to three-element-co-doped turbostratic graphene were successfully synthesized without any catalyst. Compared with heteroatom-doped graphene prepared using conventional methods, heteroatom-doped, turbostratic graphene showed lower defect levels and was free from metallic impurities.[12] Machine learning was also applied to understand and optimize this method. The choice of precursor, charge density, and other reaction parameters were mapped against the percentage of amorphous
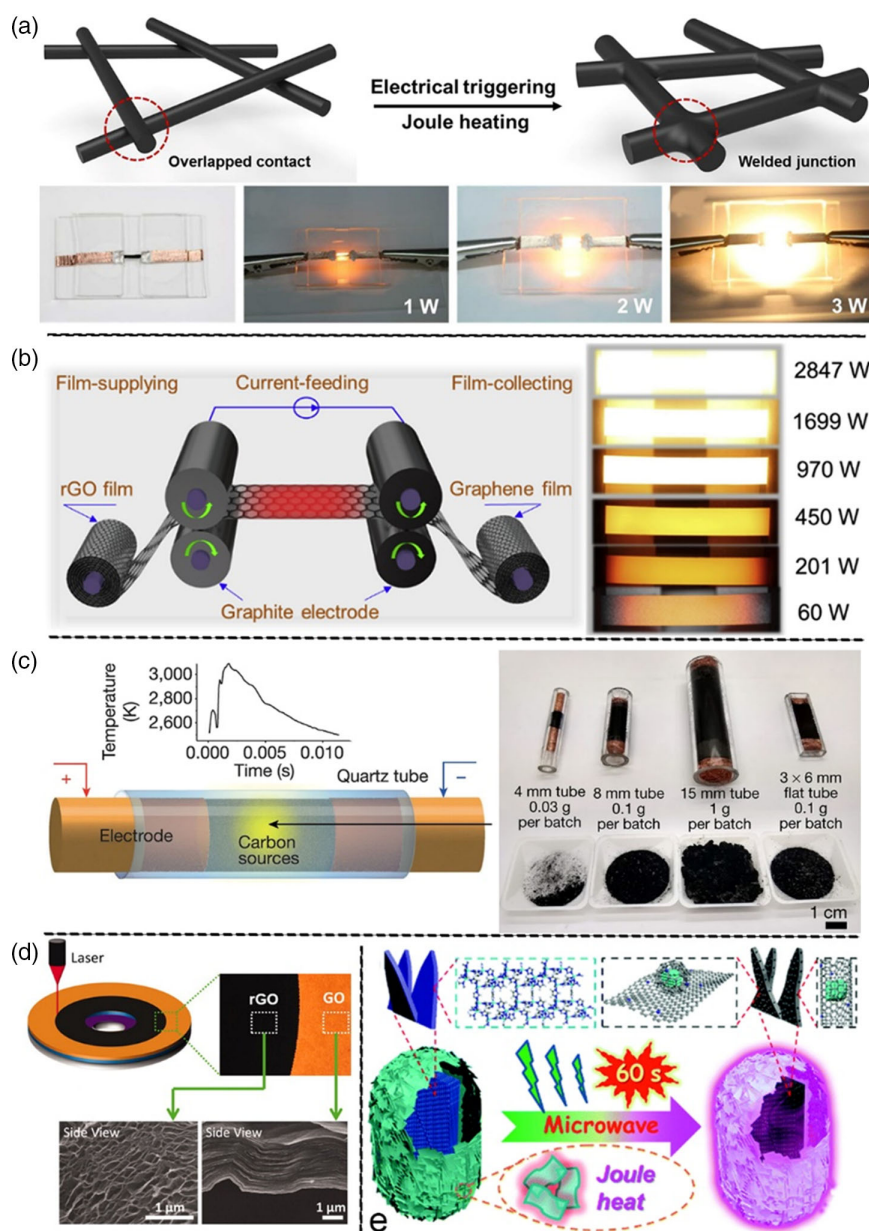
ADVANCED
SCIENCE NEWS
www.advancedsciencenews.com

small
structures
www.small-structures.com

Figure 1. a) Schematic illustration (top) of welding of carbon fibers by Joule heating and photos (bottom) showing the heating device. Reproduced with permission.[5] Copyright 2016, American Chemical Society. b) Schematic illustration of a roll-to-roll Joule heating method to produce rGO films (left) and photos of heated rGO films (right). Reproduced with permission.[7] Copyright 2019, Elsevier. c) Schematic illustration of graphene production using the Joule heating process, the temperature versus time plot (left), and photos of devices in different sizes filled with produced graphene materials (right). Reproduced with permission.[9] Copyright 2020, Springer Nature. d) Schematic illustration of laser irradiation to convert GO film to rGO film (top) and their scanning electron microscope (SEM) images (bottom). Reproduced with permission.[16] Copyright 2012, American Association for the Advancement of Science. e) Schematic illustration of microwave irradiation converting MOF/graphene mixture into carbon-supported catalysts. Reproduced with permission.[26] Copyright 2020, Royal Society of Chemistry.

carbon that was graphitized (graphene yield) and the crystallinity of the final carbon material. The charge density was found to be the most crucial parameter in controlling the graphene yield. Carbon precursors can significantly affect the crystallinity of flash graphene. A critical energy density at $100–120\,C\,g^{-1}$ was proposed, above which the heating was kinetically (diffusion)-limited, allowing additional control of graphene's crystal size.[13]

2.2. Laser Irradiation

A laser beam can generate a high-temperature spot on the surface of solid material, high enough for carbonization/graphitization. The peak temperature at the irradiated site is determined by the laser beam power, laser light absorbability, thermal conductivity of the solid material, and local gas/liquid environments.

Laser irradiation has two advantages. Rapid heating and cooling can be readily achieved by switching the laser beam on and off. Compared with other ultrafast heating methods, laser irradiation can achieve more precise controls of the heating sites due to the small size of laser beams, making it possible to create microscale patterns.[14] The drawbacks of laser irradiation methods are the high instrumental cost and the limited penetration depth of laser beams in solid precursors.

The Fourier heat transfer equation can be used to describe laser-induced pulsed heating as well as the flashlight-induced pulsed heating introduced in the next section.[15]

$$\frac{\partial^2 T}{\partial x^2} + \frac{I_1 \delta}{k} e^{-\delta x} = \frac{1}{\alpha} \frac{\partial T}{\partial t} \tag{3}$$

$$I_1 = (1 - r_f)I_0 \tag{4}$$

where I_1 is the laser intensity (W m^{-2}), t is the pulse duration (s), k is the thermal conductivity (W m^{-1} K^{-1}), α is the thermal diffusivity (m^2 s^{-1}), δ is the adsorption coefficient (m^{-1}), r_f is the reflection coefficient, I_0 is the peak power intensity (W m^{-1} K^{-1}), x is the distance from the surface subject to the laser irradiation (m), and $\partial T/\partial t$ is the heating rate (K s^{-1}).

Two innovative studies revealed new research directions on using laser irradiation to create novel carbon structures. In 2012, El-Kady et al. used an infrared laser (788 nm and 5 mW) to write directly on graphene oxide (GO) films. The heat generated under the laser spot reduced GO films, and the resulting rGO films exhibited porous structures with significantly improved electrical conductivity (Figure 1d).[16] Many other researchers have adopted this method to create various rGO patterns, which were further used to explore energy storage and sensor applications. Later in 2014, Lin et al. used a CO$_2$ laser with a much higher power (10.6 μm, 2.4–5.4 W) to directly convert polyimide (PI) film into turbostratic graphene at temperatures over 2773 K. Conventional heating at 1073–1773 K would only convert PI films to glassy carbon. The presence of aromatic and imide-repeating units in PI was found to be essential for graphitic structure formation, as they produce empty sites to host new C—C covalent bonds. The electrical conductivity of laser-induced graphene from PI was higher than that of the previously reported laser-reduced rGO, suggesting a higher graphitic level.[17] The graphitization of other precursors without these aromatic structures requires two-step irradiations. Laser irradiation is started at low temperature that converts the precursors into amorphous carbon, followed by the second laser irradiation at a much higher temperature for graphitization.[18] Carbon structures with different porosity and electrical conductivity have been fabricated using appropriate carbonaceous precursors, laser input power, and exposure duration combinations.[19] 3D structures have also been created by assembling multiple laser-irradiated 2D layers.[14]

2.3. Light Irradiation

Other than lasers, many intensive light sources, such as xenon lamps, UV lamps, and even conventional camera flashlight lamps, have been used to heat carbon precursors via photothermal effects. This approach has been extensively studied for reducing GO to rGO. Like laser irradiation, intensive light irradiation can reduce GO in milliseconds, resulting in rGO with tunable structures, porosities, and increased electrical conductivity. Light irradiation-induced ultrafast heating can synthesize hybrid materials on rGO substrates when coupled with appropriate GO pretreatments. Although the lower-energy intensity of flashlight irradiation may result in a lower heating rate than that of the laser irradiation method; a key advantage of light irradiation is that it can be realized on a much larger irradiation area than laser irradiation, making it more suitable for scalable material synthesis. Further, the instrument cost for light irradiation is much lower than that of laser irradiation. Here, we highlight several representative studies among recent works. In 2015, Wang et al. used a camera flashlight to reduce GO to make rGO thin-film electrodes. Supercapacitors assembled using these electrodes delivered a high power density of 7×10^5 W kg^{-1}.[20] Recently, Zhang et al. used a high-power flash pulse to create instant high temperature in GO/MnO$_2$ composites. The reduction of oxygenated groups in GO released reductive gases, such as H$_2$ and CO, which reduced MnO$_2$ to MnO. The resulting rGO/MnO hybrid has a high density of homogeneously distributed MnO nanoneedles in 3D rGO networks, delivering a high specific capacitance of 1706 F g^{-1}.[21] Importantly, flashlight irradiation creates different structures than conventional heating methods. For example, Ambade et al. used flashlight irradiation to fabricate mesoporous ultrathin NiO nanosheets supported on carbon cloth. Compared with NiO prepared by traditional heating methods, the flashlight irradiation-derived NiO nanosheets have a unique mesoporous structure, providing a higher surface area and more open channels.[22]

2.4. Microwave Irradiation

Microwave irradiation applies a rapidly alternating electromagnetic field to conductive materials, which drives fast electron movement, generating local Joule heating. This method has long synthesized various metal nanoparticles and carbon/metal hybrids.[23] Compared with conventional heating methods, microwave heating is usually faster, more energy efficient, and can be switched between on and off states more rapidly. However, the precise control of heating effects by microwave irradiation is difficult because the rapidly alternating electromagnetic field is hard to control, and the interactions between microwave and conductive materials are also complex.

The microwave-induced ultrafast heating can be described based on the strength of the microwave field, the frequency of the microwave, the dielectric properties, specific heat capacity, and density of carbon material, as shown in the following equations.[24]

$$P_V = \pi f \varepsilon_0 \varepsilon_r'' |E|^2 \tag{5}$$

$$\frac{dT}{dt} = \frac{P_V}{C_P \rho} \tag{6}$$

where P_V is the volumetric energy density generated during microwave heating (W m^{-3}), f is the frequency (Hz), ε_0 is the permittivity of free space/vacuum (8.85×10^{-12} F m^{-1}), ε_r'' is the dielectric loss factor, E is the field strength (V m^{-1}), C_P is the

the specific heat capacity ($J K^{-1} kg^{-1}$), ρ is the density ($kg\,m^{-3}$), and dT/dt is the heating rate ($K\,s^{-1}$).

Several representative studies include the following. In 2019, Chen et al. converted GO to ultrathin and defective carbon platelets under microwave irradiation in a microwave oven (900 W).[25] This method also allows the incorporation of ultrafine, uniformly dispersed metal/metal alloy nanoparticles into carbon. In 2020, Huang et al. exposed a carbon fiber-supported metal–organic framework (MOF) mixed with randomly stacked graphene powder to microwave irradiation (800 W).[26] In less than 60 s, the temperature went over 1273 K. The resulting carbon composite catalyst has a high yield of 48.7 wt%. It requires 0.37% energy consumption compared with traditional pyrolysis methods (Figure 1e). Later, in 2021, Zhong et al. deposited metal nanoparticles onto the surface of carbon fiber clothes by heating metal salts-coated carbon fiber clothes to 1500 K within 5 s by 900 W microwave heating.[27] The resulting composite showed good performance as the anode in Li metal batteries.

3. Carbon Structures

The unique structure of carbon atoms allows them to bond with each other in different hybridization types, resulting in diverse carbon structures. Carbon materials with different short-range or long-range atomic structures, such as graphene, CNTs, CNFs, and hard carbon, have been widely used in various applications. As discussed earlier, ultrafast heating methods have created some novel carbon structures with unique properties. In the following subsections, we will discuss several types of carbon structures created by ultrafast heating methods, including graphene, rGO, CNT architectures, hard carbon, and other carbon hybrids. Our discussion focuses on the unique ultrafast heating methods used in their syntheses, such as heating conditions and carbon precursors. Special attention was given to the capability of these methods in tailoring carbon structures. The critical properties of resulting carbon structures and demonstrated applications are summarized in **Table 1**.

3.1. Graphene

Graphene is a 2D carbon material that contains a single layer of carbon atoms arranged in hexagonal/honeycomb structures. The unique structure of graphene induces exceptional properties, making it attractive for energy storage, sensors, and structural reinforcement applications. Graphene is commonly obtained by top-down mechanical exfoliation of graphite or graphite oxide, bottom-up synthesis by chemical vapor deposition (CVD) from gaseous carbon precursors on various substrates, and thermal or chemical reduction of GO. The current synthesis methods have tradeoffs among defect density, thickness uniformity, lateral size, purity, yield, and cost.[28] Different ultrafast heating methods have been explored to synthesize unique pristine graphene structures.

Several studies focused on using laser irradiations to promote the epitaxial growth of graphene by thermal decomposition of SiC. Unlike conventional heating methods, laser irradiation results in a confined high-temperature region near the incident site on the surface, while the bulk of SiC remains close to room temperature. This feature enables the production of self-supported epitaxial graphene layers that can be directly integrated into microelectronics.[29] As discussed earlier, Tour's group reported a series of experiments to synthesize graphene films and fibers using laser-induced ultrafast heating of PI films.[17,19,30] By controlling laser irradiation process parameters, the chemical composition, surface hydrophobicity, and thickness of the resulting graphene films can be finely tuned for applications such as artificial tissues and microelectronics (**Figure 2**a). However, due to limited laser irradiation areas, it remains challenging to use laser irradiation-based ultrafast heating methods for the bulk synthesis of graphene.

Common graphene CVD synthesis often requires costly, high-purity gas precursors, flat and clean substrates (e.g., Cu, quartz, or glass), as well as high-temperature furnaces. The slow formation of graphene structures limits the production yield. Post-treatment is often needed to separate graphene from the substrate. As mentioned before, Tour's group demonstrated the syntheses of turbostratic graphene from a range of amorphous carbonaceous precursors, such as carbon black, calcined petroleum coke, coffee grounds, and anthracite coal, by the flash Joule heating method.[9,10] For precursors with a high carbon content (e.g., carbon black), the graphene production yield can reach 80%–90%, with a low defect level that is confirmed by the Raman $I_{2D/G}$ ratio up to 17. It should be noted that Raman spectroscopy is a powerful tool for the characterization of carbon materials, especially for determining their graphitic levels. For more information, we recommend reading the publications by Ferrari et al.[31] Due to the short heating time, the energy consumption of graphene production can be greatly reduced to $7.2\,kJ\,g^{-1}$. Unlike typical AB-stacked graphene obtained from graphite, turbostratic graphene with rotational mismatches (Figure 2b) permits efficient exfoliation. For example, they can be easily dispersed in water/surfactant (Pluronic F-127) with a high concentration ($4\,g\,L^{-1}$), making them readily processable for different applications. Another fast heating method used to improve the CVD synthesis of graphene is based on xenon lamp heating.[32] A single-flash irradiation can heat the metal substrate temperature to over 1773 K in 15 ms, corresponding to a heating rate of $10^6\,K\,s^{-1}$. C_2H_2 quickly decomposed on heated Ni thin films (30 nm), carbon was deposited on a quartz substrate, and carbon fragments grew into a multilayer graphene. The flashlight can heat a much larger surface than lasers, which increases the scalability of synthesis.

3.2. Reduced Graphene Oxide

rGO is produced by chemical or thermal reduction of GO with relatively low manufacturing costs. rGO still contains O and other heteroatom-containing functional groups, which are not entirely removed during reduction, resulting in varied electrical conductivities and hydrophobicity.[33] Chemically reduced rGO films or fibers typically have electrical conductivities of around $100\,S\,cm^{-1}$. Ultrafast heating methods have been used to synthesize novel rGO structures, targeting to improve the properties of rGO in several areas.

First, ultrafast heating methods have been used to induce high-temperature annealing to yield rGO films or fibers with

Table 1. Summary of representative carbon structures created using ultrafast heating methods since 2015.

Carbon structures	Precursors	Heating method	Peak T [K]	Heating rate [K min⁻¹]	Heating period	Properties				Quality				Key application reported		Ref.
						Conductivity/ Resistivity	Strength [MPa]	Young's Modulus	SSA $[m^2\,g^{-1}]^{a)}$	C purity	Other elements	D/[G] ratio	2D/[G] ratio	Devices	Key performance	
Graphene																
Graphene	4H-SiC wafer in Ar	Laser irradiation (XeCl, 1653 mJ cm⁻²)	3100–4000	–	30 ns per pulse, 300 pulses	–	–	–	–	–	Si	–	–	–	–	[29c]
Graphene	6H-SiC wafer in Ar	Laser irradiation (633 nm, 5 mW)	3600	–	4 s, 3–4 times	–	3100	–	–	–	Si	–	>1	–	–	[29d]
Graphene	Polyimide in O₂, air, Ar, H₂, SF₆	1060 nm laser (75 W)	–	–	1000 pulses in⁻¹, 15 cm s⁻¹	–	–	–	–	>86%	O, H, F, S	0.6–0.8	0.55–0.7	Hydrophobicity	Contact angle 0°–150°	[30a]
Graphene fiber	Polyimide	Laser (1060 nm, 75 W) irradiation	–	–	>40 J cm⁻²	100–200 Ω sq⁻¹	–	–	70.3	–	4.2% O 1.1% N	–	0.8	Micro-supercapacitor	10 mF cm⁻² @ 1 mA cm⁻²	[30b]
Turbostratic graphene	Amorphous carbon	Joule heating	≈3000	–	<100 ms	–	–	–	–	80%–99%	–	–	17	Bulk graphene synthesis	Energy consumption: 7.2 kJ g⁻¹	[9]
Turbostratic graphene	Plastic waste	Joule heating	≈2900	–	8 s	–	–	–	–	–	–	–	6	Plastic waste recycling	Energy consumption: 23 kJ g⁻¹	[11a]
Graphene	Ni film in C₂H₂/ Ar/H₂	Xenon flashlight irradiation	≈1773	–	15 ms, 30 J cm⁻¹	3.272 × 10³ Ω sq⁻¹	–	–	–	–	–	–	0.65	–	–	[32]
rGO																
rGO film	Freeze-dried GO film	Camera flashlight irradiation	–	–	–	60.7 S m⁻¹	–	–	733	–	21% O	–	–	Supercapacitor	7 × 10⁵ W kg⁻¹ 50% retention @ 220 A g⁻¹	[20]
rGO film	GO film	Xenon flashlight irradiation	–	–	20 ms, 40 J cm⁻²	17.55 Ω sq⁻¹	–	–	–	96%	–	–	–	–	–	[34]
rGO film	GO	Joule heating	2750	–	1 min	3112 S cm⁻¹ 0.8 Ω sq⁻¹	20.1	–	–	C/O = 81.64	O	1.02	0.93	Current collector in Li-ion battery	110 mAh g⁻¹ @ 7 C g⁻¹	[35]
rGO film	GO	Joule heating	1473 & 2673	–	20 min	4200 S cm⁻¹ 1285 ±20 W m⁻¹ K⁻¹	16.7	320	–	98%	O	0.08	0.97	–	–	[7]
rGO fiber/ film/foam	GO	Joule heating	≈2000	–	–	0.28 Ω (contact resistance)	–	–	–	C:O = 21.3	O	0.08	–	–	–	[36]
rGO fiber	GO	Joule heating	>2273	–	–	1020 S cm⁻¹	–	–	–	98%	O	0.15	–	–	–	[37]
rGO fiber	GO	Joule heating	≈3000	–	50 s	2721 S cm⁻¹	141.2	19 000	–	–	–	0.18	–	Current conductor	3.84 × 10⁴ A cm⁻² 4.67 × 10⁴ A cm g⁻¹	[38]

Table 1. Continued.

Carbon structures	Precursors	Heating method	Peak T [K]	Heating rate [K min⁻¹]	Heating period	Properties				Quality				Key application reported		Ref.
						Conductivity/ Resistivity	Strength [MPa]	Young's Modulus	SSA [m² g⁻¹]ᵃ⁾	C purity	Other elements	D/[G] ratio	2D/[G] ratio	Devices	Key performance	
rGO	GO	Flashlight irradiation	≈1000	–	–	$3.5\,S\,m^{-1}$	–	–	267.81	C/O = 6.02	14.24 at % O	–	–	Supercapacitor	Capacitance: $166.7\,F\,g^{-1}$ @ $0.5\,A\,g^{-1}$	[39]
rGO foam	GO	SPS	473–673	–	2–3 min	–	40	4.1	–	–	O	0.6	–	Bone implant	–	[40]
N-doped rGO	GO, melamine	Flashlight irradiation	1773	–	5 ms, $1.5\,kJ\,cm^{-2}$	–	–	–	594.64	26 % N	N, O	0.7	0.025	Anode of Li-ion battery	$1225\,mAh\,g^{-1}$ @$0.5\,A\,g^{-1}$	[41]
rGO/GO film	GO	Camera flashlight	–	–	1 ms	–	–	–	–	C/O = 5.18	O	1.19	–	Humidity sensor	1 s response (11%–95% RH) 24 s recovery	[44a]
rGO/GO film	GO	Camera flashlight irradiation	–	–	–	–	–	–	–	C/O = 11.7 (rGO), 2.65 (GO)	O	–	–	Humidity actuator	16 s response, 17 s Recovery (86% RH)	[44b]
rGO/GO fiber	GO	Xenon flashlight irradiation	1073	–	0.66 ms	$15.2\,S\,cm^{-1}$	133	–	–	C:O = 4	O	0.84	–	Humidity sensor	Response time in mins, 99.9% RH	[45]
rGO/ graphene film	GO, graphene, SnSO₄	Camera flashlight irradiation	–	–	1 s, 3 times	–	–	–	–	rGO/ graphene=2/ 1	Sn	0.36	–	Anode for Na ion battery	$615\,mAh\,g^{-1}$, >84% retention over 50 cycles	[46]
Hard carbon																
Hard carbon	Switchgrass	Joule heating	2323	–	–	$25.86\,S\,cm^{-1}$	–	–	–	92%	–	1.04	0.76	Anode in Na ion battery	$200\,mAh\,g^{-1}$ @ $50\,mA\,g^{-1}$ 87% capacity retention over 800 cycles	[47]
Hard carbon	Sucrose	SPS	1573	300–500	5 min	–	–	–	–	96.54%	O	2.52	–	Anode in Na ion battery	$299.4\,mAh\,g^{-1}$ @ $30\,mA\,g^{-1}$	[48]
CNT architectures																
Welded CNTs	CNTs	Joule heating in TEM	3500	–	1 ns	36.1 kΩ	24 000	–	–	–	–	–	–	–	–	[52]
Welded CNTs	CNTs	Joule heating in TEM	2300	–	–	$1000\,S\,cm^{-1}$	–	–	–	–	–	0.16	–	–	–	[53]
CNF film	CNF film	Joule heating	>2500	200	10 min	$381\,S\,cm^{-1}$	3.86	–	–	97.08%	O-2.55%, N-0.37%	0.035	–	–	–	[5]
CNT fiber network	CNT fibers, ethanol	Joule heating	2273	–	–	4.8 Ω	$0.47\,N\,tex^{-1}$	–	–	–	–	1.11	–	–	–	[55]
CNT film	CNTs, polyacrylonitrile	Joule heating	>2800	–	30 min	$1500\,S\,cm^{-1}$	120	–	–	–	–	0.1	–	–	–	[6]
CNT/C fiber	CNT, polyacrylonitrile	Joule heating	1800	–	2–15 s	$4700\,S\,cm^{-1}$	2300	–	–	–	–	–	–	–	–	[56]

ADVANCED
SCIENCE NEWS

www.advancedsciencenews.com

small
structures

www.small-structures.com

Table 1. Continued.

| Carbon structures	Precursors	Heating method	Peak T [K]	Heating rate [K min⁻¹]	Heating period	Properties				Quality				Key application reported		Ref.
						Conductivity/ Resistivity	Strength [MPa]	Young's Modulus	SSA [m² g⁻¹]ª⁾	C purity	Other elements	D/[G] ratio	2D/[G] ratio	Devices	Key performance	
Other carbon hybrids																
RGO/CNT paper	GO, CNTs	Joule heating	3320	–	–	240 000 S m⁻¹				–	–	–	–	Lightning	90% of input as radiation output	[57]
Graphene/CNT film	CNTs, graphene	SPS	1473	150	7 min	108 S cm⁻¹ [55 S cm⁻¹]	–	–	–	–	–	–	–	–	–	[58]
RGO/CNT paper	GO, CNTs	Camera flashlight	–	–	1 h	–	–	–	–	–	–	–	–	Surface hydrophobicity	Contact angle: 120°	[59]
RGO/CNT film	GO, CNTs	Joule heating	2936	–	1 min	2750 S cm⁻¹	–	–	–	C/O = 3.3	O	0.14	–	Current collector in Al ion battery	106.1 mAh g⁻¹ @ 0.2 A g⁻¹, 99.5% retention after 150 cycles	[60] ch
CNT/carbon fiber	CNTs, carbon fibers, epoxy	Laser irradiation (Nd:YAG, 6 W)	–	–	200 mm s⁻¹	–	45.02	–	–	–	–	–	–	–	–	[56]
CNT/AC CNT/rGO	Carbonized woodblock rGO film	Joule heating	2457	–	1 min	–	–	–	–	–	–	–	–	–	–	[61]
CNT/glass fiber	CNTs, glass fibers	Joule heating	1273	>60 000	<1 s	0.612 S cm⁻¹	1190	34 500	–	–	–	–	–	Structural heater	–	[62]

ª⁾SSA: specific surface area.
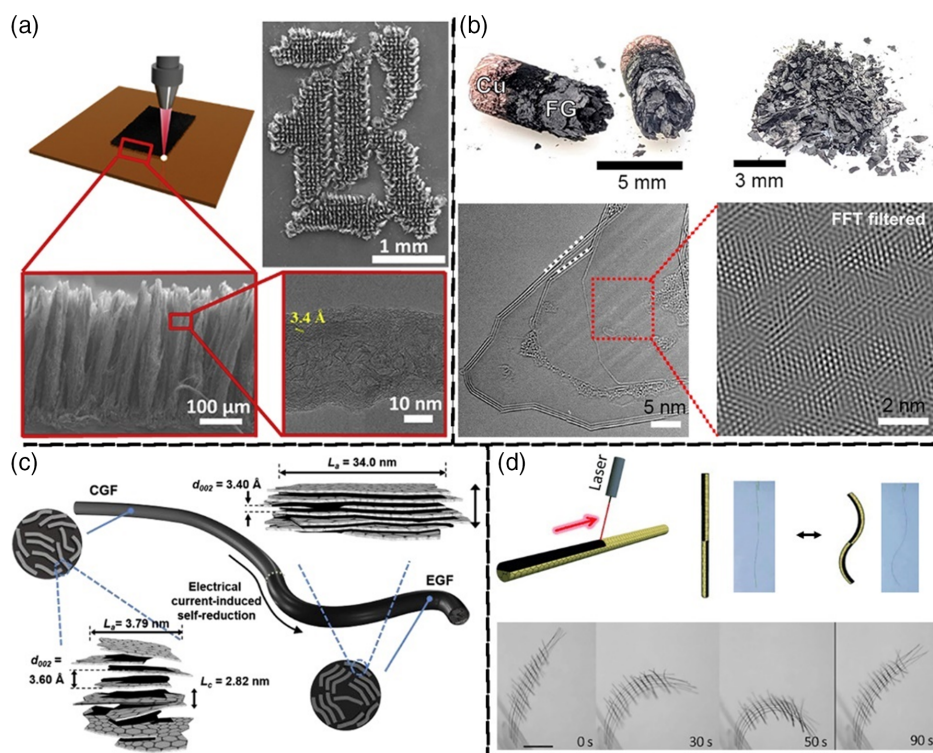
Figure 2. a) Schematic illustration of laser writing on PI film, a photo of an "R" shape pattern, and SEM images of graphene fibers. Reproduced with permission.[30b] Copyright 2018, Elsevier. b) Photos of turbostratic graphene and Cu wool used as an electrode (top) and transmission electron microscope (TEM) images of graphene sheets with a rotational mismatch and a moiré pattern (bottom). Reproduced with permission.[10] Copyright 2020, Springer Nature. c) Schematic illustration of structural evolution of chemically reduced GO fibers under Joule heating treatment. Reproduced with permission.[37] Copyright 2018, Elsevier. d) Schematic illustration of positioned laser reduction on different regions of GO fibers (top left), photos of the reversible response of an rGO/GO hybrid fiber when exposed to moistures (top right), and a responsive textile exposed to an 80% relative humidity environment at different exposure times (bottom). Reproduced with permission.[42] Copyright 2013, Wiley-VCH GmbH.

significantly improved electrical conductivity. As discussed earlier, El-Kady et al. used laser irradiation to create fast local heating, reducing GO films into rGO films with an improved conductivity of 17.38 S cm^{-1}, much higher than that of activated carbon (0.1–1 S cm^{-1}) commonly used in commercial supercapacitors.[16] Besides laser irradiation, flashlight irradiation has also been used in several studies to reduce GO films into rGO films.[20,34] In 2016, Chen et al. applied Joule heating to reduce GO film at temperatures up to 2750 K in 1 min. The high-temperature treatment effectively removed functional groups, improved graphitic crystallinity, and densified the packing of graphene layers, resulting in a drastically improved electrical conductivity of 3112 S cm^{-1}.[35] The authors also used Raman spectroscopy to characterize the rGO films and demonstrated their highly crystalline structure with a decreased I_D/I_G ratio and a high I_{2D}/I_G ratio of 0.93. These rGO films were used as current collectors in Li-ion batteries. As previously introduced, the Joule heating reduction method can be further scaled to a high-throughput roll-to-roll process to convert chemically reduced rGO films into graphene films.[7] By Joule heating, Liu et al. also showed that various rGO fibers, films, and foams could be covalently welded together to form GO films.[36] In 2019, Noh et al. applied a similar Joule heating method on chemically reduced rGO fibers. As illustrated in Figure 2c, the fast heating

restores large sp^2 crystallite domains, reduces the interlayer spacing between graphene layers, and induces the alignment of crystallite domains along the direction of the electrical field. The large sp^2 crystallite domains also facilitate charge hopping transport along the lateral plane of rGO. The treated rGO fibers showed a high electrical conductivity of around 1000 S cm^{-1}.[37] A recent study applied a two-step Joule heating on GO fiber, which pushed its conductivity to 2721 S cm^{-1}. The rGO fiber showed a specific current-carrying capacity of 4.67×10^4 A cm g^{-1}, higher than that of commercial Cu wire.[38]

The second area concerns creating rGO structures with appropriate surface properties, porosity, and mechanical properties required by specific applications. Compared with the first area, much lower temperatures were used to prevent the stacking of rGO nanosheets. For example, a recent systematic study on GO film reduction by flashlight irradiation found that O content in rGO films benefits redox reactions, contributing to higher specific capacitance (166.7 F g^{-1}) than more extensively reduced films.[39] For supercapacitor applications, mild flashlight irradiation on GO films may yield better performance. Chakravarty et al. used spark plasma sintering (SPS) to induce fast localized Joule heating at 473–673 K, which welded rGO nanosheets into porous 3D scaffolds for biological applications.[40]

The third area is to control the heteroatom doping of rGO. For example, N doping can yield interesting electrochemical properties of carbon materials with many applications in electrocatalysts and energy storage devices. However, because C—N bonds are unstable at high temperature, N doping by conventional heating methods usually has a low N doping level (e.g., less than 10 at%). Yoo et al. reported using ultrafast heating to increase the N doping level in rGO using an intense pulsed light from a Xenon lamp.[41] The light irradiation raised the temperature of solid powder containing GO and melamine to 1773 K in 3 ms, resulting in N-doped rGO with a high N content of 26 at%. The authors proposed that the high N content was achieved because of the effective decomposition of melamine near the graphene surfaces at high temperatures, abundant interactions between N atoms and graphene, and fast structural relaxation by thermal quenching. The N-doped rGO was applied as an anode material for Li storage.

The fourth area is related to the formation of rGO/GO hybrid structures. Due to their different surface functional groups, rGO and GO have significantly different hydrophobicity. rGO/GO hybrid structures can have reversible and controllable shape changes in response to environmental stimuli. Water exhibits a stronger affinity to O-rich GO layers than rGO. Cheng et al. used a laser beam to partially reduce GO fibers, resulting in rGO/GO hybrid fibers.[42] As shown in Figure 2d, this asymmetric fiber can behave as a moisture-sensitive actuator when exposed to water vapor. This property was explored to create novel moisture-responsive actuators, textile, and walking robots by rationally selecting and locating laser-induced rGO regions along GO fibers. Several other teams have also carried out research using similar approaches. Han et al. used focused sunlight to create a moisture-responsive rGO/GO paper.[43] Light irradiation by flash lamps has also been used to reduce GO and fabricate moisture sensors and moisture-responsive actuators.[44] A recent study has explored rGO/GO hybrid fibers prepared by flashlight irradiation as humidity sensors.[45] In addition, the porosity and mechanical properties of rGO/GO hybrids can be tuned by changing the ratio between rGO and GO due to their significantly different mechanical properties. Jeon et al. used flashlight heating to reduce the mixture of GO and graphene. They controlled the properties of the resulting rGO/GO/graphene hybrid by the irradiation conditions and the mixing ratio between GO and graphene.[46] The porous hybrid was used to host Sn nanoparticles and worked as an efficient anode in Na-ion batteries.

3.3. Hard Carbon

Hard carbon refers to carbon materials that cannot be converted to graphite by high-temperature treatments. They are usually produced by direct heating or hydrothermal carbonization of sugars, biomass, or polymers, followed by a further pyrolysis treatment at 1000–1873 K over several hours. They have been considered promising anode materials for alkali metal-ion batteries. Two studies have used ultrafast heating methods to produce hard carbon, showing good performance in battery applications. In 2017, Zhang et al. used Joule heating to carbonize switchgrass at 2323 K, making hard carbon with 3D hierarchical pores. Due

to the much higher carbonization temperature than standard carbonization methods, the average interlayer spacing among graphene layers in this hard carbon was 0.376 nm with decreased specific surface area. The initial Coulombic efficiency and rate capability of assembled Na-ion batteries were improved.[47] Recently, Zhen et al. reported an SPS method (**Figure 3**a), which combines plasma activation, hot pressing, and Joule heating to achieve a heating rate of 300–500 K min^{-1}.[48] The hot pressing compressed various carbon precursors, such as sucrose, fructose, and glucose, under high pressure (20 MPa). Then, Joule heating at 1373 K between 1 and 0 min was applied to convert them to hard carbon with fewer defects, lower porosity, and less O content than traditional heating methods. The resulting hard carbon showed improved initial Coulombic efficiency of 88.9%, a high reversible capacity of 299.4 mAh g^{-1}, and a high rate capacity of 136.6 mAh g^{-1} at 5 A g^{-1} as anode materials in Na-ion batteries.[48]

3.4. CNT Architectures

CNTs with sp^2 carbon atoms in unique 1D tubular structures have many exceptional properties. Assembling CNTs into 2D/3D architectures can create opportunities for many new applications. However, assembled CNTs with weak van der Waals forces often fails to translate the intrinsic properties of CNTs into the resulting architectures. For example, the electrical conductivity of individual CNTs can reach 10 000 S cm^{-1}, while that of CNT films assembled by van der Waals forces is usually around 100 S cm^{-1}.[5] Heating treatment may enhance the interactions between CNTs. However, standard heating methods fail to create CNT architectures with desirable properties.

Several TEM studies have demonstrated that joining individual CNTs at the nanoscale is possible. For example, Terrones et al. used electron irradiation to create high temperatures on CNTs in a TEM, introducing vacancy defects and dangling bonds in CNTs.[49] Coupled with the thermal annealing, adjacent CNTs with matching chirality and similar diameters would merge. CNTs would shrink in a vacuum under electron irradiation and simultaneous Joule heating due to carbon evaporation.[50] Jin et al. demonstrated that CNTs of similar diameters joined together when Joule heating was applied to two CNTs placed in a cap-to-cap position between a W-tip and a platinum wire counter electrode in TEM.[51] If W metal particles were presented as catalysts, CNTs in different diameters could be joined together. A recent study in TEM showed that controlled Joule heating could crystallize amorphous carbon deposited at the gap between two CNTs into a multilayer tubular structure and merge into CNTs.[52] Gong et al. also showed that CNTs fuse via graphitic carbon bonds when heated to 2300 K by Joule heating in TEM, leading to three orders of increase in the electrical conductivity of CNT bundles.[53] These TEM experiments confirm that it is feasible to seamlessly join CNTs into various architectures at the nanoscale under proper local heating conditions. However, applying TEM methods to samples at the macroscale is impractical.

In contrast, ultrafast heating methods have shown promise in realizing macroscale assembly of CNT architectures. As discussed earlier, Joule heating was initially used to weld CNF
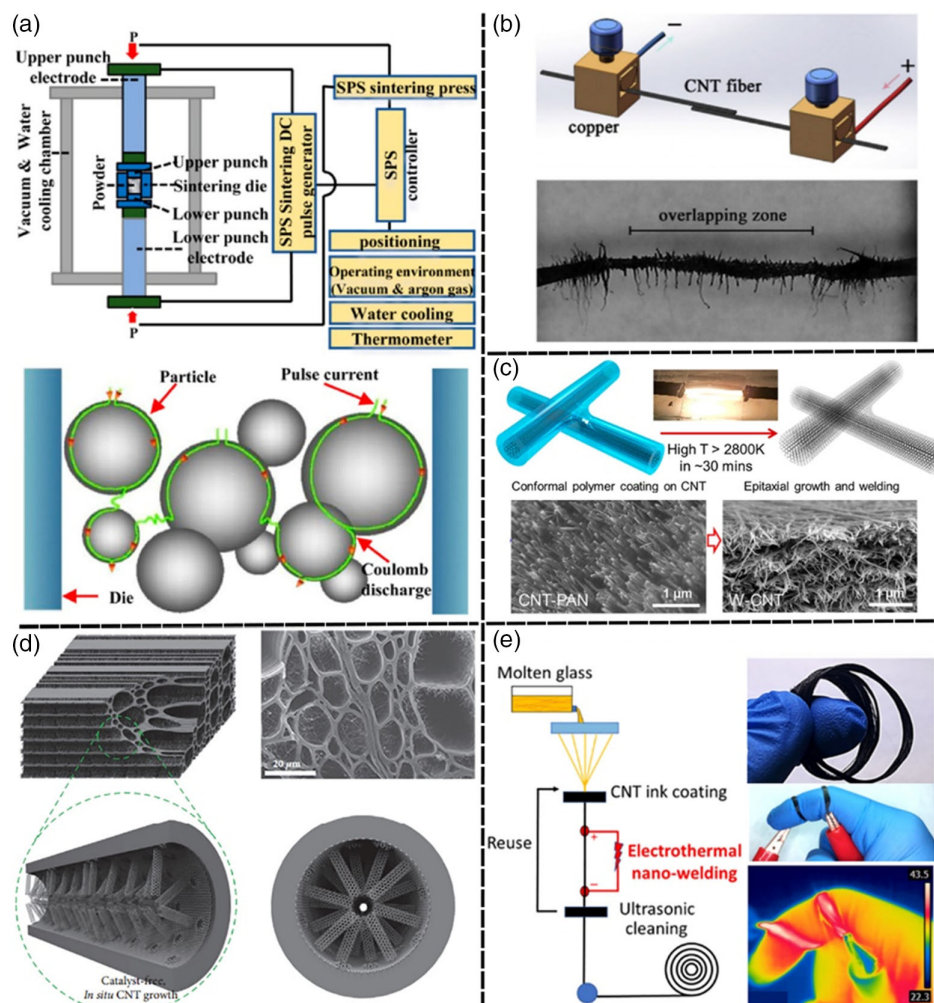
Figure 3. a) Schematic illustration of the SPS system (top) and the heating mechanism (bottom). Reproduced with permission.[48] Copyright 2022, National Academy of Sciences. b) Schematic illustration and photo of the soldering of two overlapped CNT fibers. Reproduced with permission.[55] Copyright 2017, Elsevier. c) Schematic illustration of polymer-coated CNTs welded via ultrafast heating and a photo of the heated CNF film (top) and SEM images of CNTs before and after welding (bottom). Reproduced with permission.[6] Copyright 2018, American Chemical Society. d) Schematic illustration and an SEM image of CNTs formed inside confined spaces of carbonized wood. Reproduced with permission.[61] Copyright American Association for Advancement of Science. e) Schematic illustration of a roll-to-roll process to produce welded CNT/glass fibers (left), two photos, and an IR image of heated CNT/glass fibers (right). Reproduced with permission.[62] Copyright 2020, American Chemical Society.

networks.[5] The O and N functional groups/defects within the amorphous carbon content in CNFs were removed through gasification by ultrafast heating, generating bonding sites for the formation of new graphitic C—C bonds for more effective interconnections in 3D architectures. The welding may take place between both crossover and parallel CNFs. The former resulted in the formation of 3D architectures, whereas the latter resulted in merging parallel CNFs into larger CNF bundles with various diameters.[5] For highly crystalline pristine CNTs, there is insufficient amorphous carbon content to produce reactive carbon species required to readily weld CNTs together; thus, soldering is preferred over welding. However, metal solders that could be used for welding carbon materials (e.g., Ti, Cr, Fe, Au, Pt, and Pd) usually have either poor wettability with CNTs or large contact resistances.[54] Thus, amorphous carbon was used as the

solder to join CNTs. Zou et al. used Joule heating to join CNT fibers in a CVD reactor. As shown in Figure 3b, the electrical current up to 400 mA was applied through CNF fibers. Ethanol was introduced to deposit as amorphous carbon at local contact joints between CNT fibers where the temperature was higher due to larger contact resistance. The CNT fibers' linear resistance decreased from >120 to $4.8\,\Omega$ after deposited amorphous carbon aggregated into carbon clusters without damaging the structure of CNT fibers.[55] Besides using gaseous carbon precursors to deposit amorphous carbon, CNTs can be coated with graphitizable polymers that can be converted to graphitic carbon structures under ultrafast heating to weld CNTs together. As briefly described in the previous section, Yao et al. reported that Joule heating enabled welding on CNTs via an "epitaxial welding process." Polyacrylonitrile (PAN) was dip coated onto CNTs as

**ADVANCED
SCIENCE NEWS**
www.advancedsciencenews.com

**small
structures**
www.small-structures.com

the source of amorphous carbon during soldering. PAN underwent epitaxial graphitization during ultrafast heating, producing covalent C—C bonds to reinforce the interconnection between individual CNTs. The electrical conductivity of the welded CNT architectures was $2000\,S\,cm^{-1}$ compared with $314\,S\,cm^{-1}$ of the original CNT architectures. The mechanical yield strength was also improved by four times, from 5.6 to 22.5 MPa (Figure 3c).[6] A similar approach was also applied to CVD-synthesized CNT fibers. Li et al. infiltrated CNT fibers with PAN. The composite fibers were carbonized in two steps using Joule heating under tension, resulting in significantly improved mechanical properties.[56]

3.5. Other Carbon Hybrids

Ultrafast heating methods also show promising results in assembling different carbon materials into hybrids, which combine the advantageous properties of individual components. The general approach is to heat carbon materials at a high temperature so they can be welded or joined together at the nanoscale. For example, in 2016, Bao et al. reported an rGO/CNT paper composed of monolayer rGO nanosheets and 10 wt% single-walled CNTs. The GO/CNT paper was first fabricated by Mayer rod printing, spray coating, or 3D printing. The embedded conductive CNTs enable uniform current distribution under electrical bias. Under Joule heating, GO was reduced to rGO. The hybrid paper showed mechanical flexibility and high-temperature stability (at 3000 K) and was used as planar lighting elements.[57] In 2017, Nautiyal et al. welded multilayer graphene nanoplatelets (6–8 nm in thickness) with CNTs using SPS. The mixed solid powder was heated to 1473 K at $150\,K\,min^{-1}$ under 60 MPa. Testing results suggested that CNTs acting as anchors between graphene layers create electrical conduction paths. The hybrid showed improved electrical conductivity, mechanical strength, and less significant anisotropy behavior.[58] RGO/CNT hybrid films were also prepared by flashlight heating.[59] In 2020, Liu et al. used Joule heating at 2936 K to fabricate rGO/CNT hybrid films in less than 1 min. The functional groups on rGO were eliminated, and the interlayer distance of the rGO decreased from 0.367 to 0.335 nm. The electrical conductivity was increased 10^{6}-fold to $2750\,S\,cm^{-1}$. The rGO/CNT films were used as flexible current collectors in aqueous Al-ion batteries.[60] CNTs were also assembled on the surface of carbon fibers by laser irradiation.[56] Chen et al. recently used Joule heating to heat carbonized wood at 2500 K over 1 min. CNTs were formed inside confined spaces of carbonized wood (Figure 3d). It was proposed that defect sites with higher electric resistance led to local high-temperature regions. The temperature gradient drives the formation of CNTs without a metal catalyst. CNT formation was also observed between heated rGO layers.[61] Other than carbon materials, Shang et al. showed that CNTs could also be assembled with glass fibers by Joule heating. CNTs were first deposited on glass fibers from their suspension. Under Joule heating, the high resistance at CNT junctions created high local temperatures above 1273 K at a high rate $>1000\,K\,s^{-1}$, which melted glass to anchor CNTs into glass fibers. The resulting CNT/glass fibers were used as structural and functional heaters. As illustrated in Figure 3e, the Joule heating-based welding may be integrated into the industrial glass fiber manufacturing process, leading to scalable roll-to-roll CNT/glass fiber manufacturing.[62]

4. Carbon/Metal Hybrid Structures

Carbon/metal hybrids with metal nanoparticles supported on conductive carbon substrates are essential electrocatalysts in various energy storage and conversion processes. Their synthesis usually requires coating metal precursors on a suitable carbon substrate, followed by high-temperature treatments to decompose metal precursors and graphitize carbon substrates simultaneously. The size, elemental composition, and surface distribution of metal nanoparticles are significantly affected by the temperature and duration of high-temperature treatments. Low temperature would result in incomplete decomposition of metal precursors and insufficient carbon graphitization, resulting in a low yield of nanoparticles and defective carbon substrates. On the other hand, an extensive heating period at high temperatures would promote the agglomeration of nanoparticles into larger particles, resulting in poor metal particle dispersion on carbon substrates, thus reducing catalytic activity and stability. Ultrafast heating methods provide opportunities to enable the complete decomposition of metal precursors in a short period coupled with fast cooling to quench the subsequent metal agglomeration. Very high-temperature treatment may also allow the formation of alloy particles with desirable elemental compositions. In the following subsections, we will discuss recent advances in forming various carbon/metal hybrid structures, including carbon-supported monometallic nanoparticles, metal alloy or metal composite nanoparticles, HEA nanoparticles, and SACs. Their synthesis conditions, metal structures, and applications are summarized in **Table 2**.

4.1. Carbon-Supported Monometallic Nanoparticles

An early study on forming carbon-supported metal nanoparticles via the ultrafast heating method was an extension of the formation of the rGO/GO/graphene hybrid. The porous carbon film formed by the camera flash irradiation reduction was immersed in $SnSO_4$ solution, allowing Sn nanoparticles to be electrodeposited onto the carbon hybrid substrate.[46] It was found that the porous carbon substrate accommodated the large volume change of Sn nanoparticles during repeated cycling in Na-ion batteries.

In 2016, Chen et al. reported a pioneer work on creating metal nanoparticles by a direct ultrafast heating method. Si, Sn, or Al particles of a few micrometers in size were first filtered onto a freestanding rGO film. Then, the Si/rGO hybrid film was heated by radiation from a Joule-heated rGO film (**Figure 4**a). These large Si particles were transformed in situ into nanoparticles with a size between 10 and 15 nm at 1800 K in 30 s. In comparison, forming Sn or Al nanoparticles required a shorter heating period of 1 s. The mass loading of metal nanoparticles on rGO films can reach $2.5\,mg\,cm^{-2}$. These hybrid films were used as freestanding high-capacity anodes for Li-ion batteries.[63] This method was also used to synthesize Ni nanoparticles from Ni microparticles. The resulting Ni/rGO hybrid was used as catalysts in H_2O_2 fuel cells.[64]

Table 2. Summary of representative carbon/metal hybrid structures synthesized using ultrafast heating methods since 2015.

Carbon substrates	Metal precursors	Heating method	Peak temperature [K]	Heating rate [K s^{-1}]	Heating period	Metal structures	Nanoparticle size [nm]	Metal Loading [wt%]	Key application reported	Ref.
rGO/GO/graphene hybrid	SnSO$_4$	Camera flash reduction, electrodeposition	–	–	–	Sn NPs[a]	–	–	Li-ion battery	[46]
rGO	Si, Sn or Al microparticles	Joule heating	1800	–	1–30 s	Si NPs	10–15	–	Li-ion battery	[86]
rGO	Ni microparticles	Joule heating	2370	–	12 ms	Carbon-coated Ni NPs	25–100	–	H$_2$O$_2$ fuel cell	[64]
CNFs	Ag acetate	Joule heating	1600	70 000	0.1 s	Ag NPs	40	–	Li-metal battery	[65]
CNFs	PdCl$_2$	Joule heating	2100	400 000	5 ms	Pd NPs	4	–	–	[65]
rGO	NiCl$_2$	Joule heating	1900	10 000	54 ms	Ni NPs	≈5	–	Li-CO$_2$ battery	[66]
Carbon fibers, activated carbon fibers	RuCl$_3$	Joule heating	1600	36 000	44 ms	Ru NPs	9.0, 4.1	–	Li-CO$_2$ battery	[67]
CNFs, activated CNFs	Pt	Joule heating	1800	–	55 ms	Pt, Ru, Ir, Ni NPs	1-50	–	CO oxidation	[67]
Cellulose, carbon paper	CuCl$_2$, Pd, Pt, Ni salts	Joule heating	–	–	0.3–3 s	Cu, Cu-Pd, Cu-Pd-Pt, Cu-Pd-Pt-Ni NPs	35	–	CO$_2$ reduction	[68]
Carbon black	H$_2$PtCl$_6$	Joule heating	1400, 3200	Continuous process	50 ms	Pt NPs	4	–	Methanol oxidation	[69]
Ni-tartrate complex	Ni-tartrate complex	Laser irradiation	–	–	–	Ni NPs	–	–	–	[70]
GO	Co, Cu, Fe, Ni nitrates, PdCl$_2$	Microwave irradiation	–	–	–	Co, Cu, Fe, Ni, Pd, Co-Ni, Co-Ni-Cu NPs	2-40	–	–	[25]
Carbon fiber	Co-MOF Ni-MOF Fe-MOF NiCo-MOF	Microwave irradiation	>1273	–	60 s	Co, Ni, Fe, Ni-Co NPs	–	–	Water splitting	[26]
Carbon fiber, graphite flake, carbonized wood	Ni, Co, Zn, Ag, Cu nitrates	Microwave irradiation	1500	300	2–4 s	Ni, Co, Zn, Au, Cu NPs	268.6	–	Li-metal battery	[27]
CNFs	PdCl$_2$ and NiCl$_2$	Joule heating	1550	15 000	1 s	Pd-Ni alloy NPs	10-50	–	HER	[71]
CNFs	H$_2$PtCl$_6$, PdCl$_2$, HAuCl$_4$, RuCl$_3$	Joule heating	–	–	0.2 s	Pt, Pt-Pd, Pt-Au-Ru, Pt-Pd-Au-Ru NPs	500	–	Li-O$_2$ battery	[72]
GO	NiCl$_2$ and FeCl$_3$	Microwave irradiation	1273	–	2 s	metastable Ni-Fe alloy NPs	30-50	–	OER	[73]
CNFs	Si nanoparticles (70–120 nm)	Joule heating	2000	–	40 s	SiC/C necklace-like structures	10	–	–	[74]
Carbon cloth	MoO$_3$/graphene	Xenon flashlight	–	–	4 pulses at 575 V	Porous Mo$_2$C	–	–	HER	[75]
CNFs	MCl$_x$H$_y$ (M is Pt, Pd, Ni, Fe, Co, AU, Cu, or Sn)	Joule heating	2000	100 000	55 ms	HEA NPs	5.3–56.8	–	Ammonia oxidation	[8]
CNFs, rGO film, carbonized wood	PdCl$_2$, RuCl$_3$, FeCl$_3$, NiCl$_2$, CoCl$_2$, H$_2$PtCl$_6$	Microwave irradiation	1850	1000	10 s	PtPdFeCoNi HEA NPs	12	–	–	[77]
Aniline, graphene	H$_2$PtCl$_6$	Microwave irradiation	–	–	2 min	Pt SACs	–	0.44	HER	[81]
GO	H$_2$PtCl$_6$	Laser irradiation (1064 and 355 nm)	1350 and 1693	–	Scan at 1000 mm s^{-1}	Pt SACs	–	0.41	HER	[80b]

Table 2. Continued.

Carbon substrates	Metal precursors	Heating method	Peak temperature [K]	Heating rate [K s^{-1}]	Heating period	Metal structures	Nanoparticle size [nm]	Metal Loading [wt%]	Key application reported	Ref.
Activated CNFs, rGO, C$_3$N$_4$, TiO$_2$	H$_2$PtCl$_6$	Joule heating	1500	27 000	10 cycles of 55 ms + cooling	Pt SACs	–	0.24	Methane conversion	[82]
Carbon black	1,10-phenanthroline–Ni acetate, Fe, Co, Cu, Zn	Joule heating	1573	2600	0.5 s	Ni-N$_x$ SACs, Fe, Co, Cu, Zn SACs	–	–	CO$_2$ reduction reaction	[83]
Porous CNFs	Co acetate	Joule heating	1023	7500	1 s	Co NPs and Co-N-C SACs	5–7	–	ORR and OER in Zn-air battery	[84]
GO, ammonia	Cocl$_2$	Joule heating in NH$_3$	–	–	2 s	Co-N-C SACs	–	0.81	HER	[85]

a)NPs: nanoparticles.
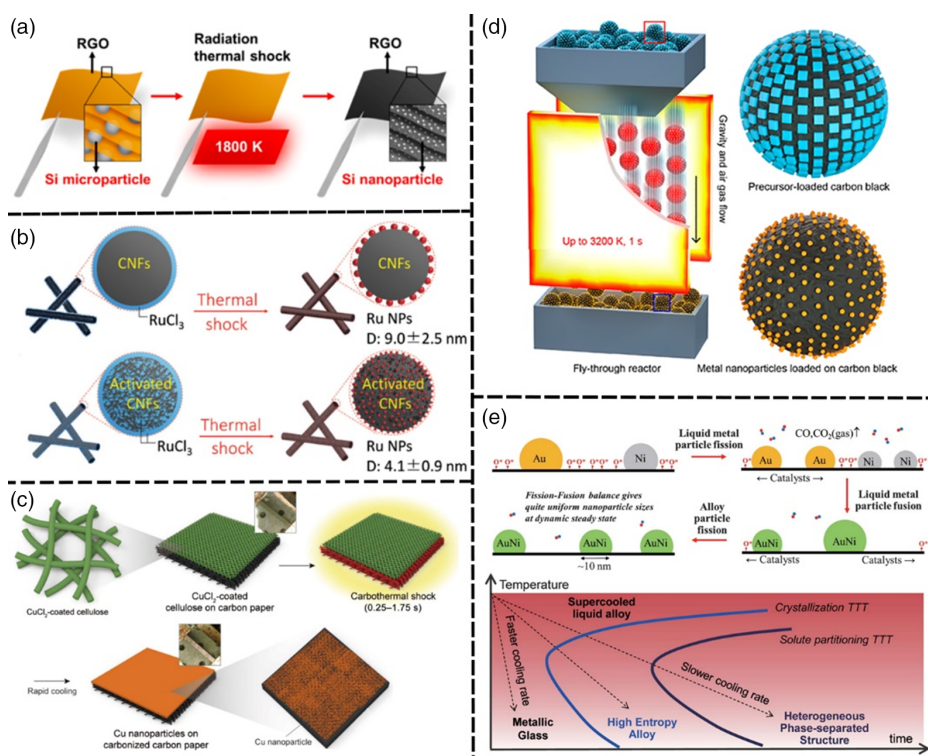
Figure 4. a) Schematic illustration of Si nanoparticle formation on rGO film using thermal radiation from Joule-heated rGO film. Reproduced with permission.[63] Copyright 2016, American Chemical Society. b) Schematic illustration of Ru nanoparticle formation on CNFs and activated CNFs.[67] Copyright 2019, American Chemical Society. c) Schematic illustration of Cu nanoparticle synthesis on carbolized carbon paper using a cellulose coating. Reproduced with permission.[68] Copyright 2021, American Association for Advancement of Science. d) Schematic illustration of the fly-through high-temperature reactor and the thermal decomposition of metal salt precursors into metallic nanoparticles anchored on carbon black. Reproduced with permission.[69] Copyright 2021, American Chemical Society. e) Schematic illustration of the catalysis-driven liquid metal droplet fission/fusion toward uniformly dispersed HEA nanoparticles (top) and time–temperature–transformation (TTT) diagram showing the kinetic formation of HEA as a function of cooling rate (bottom). Reproduced with permission.[8] Copyright 2018, American Association for Advancement of Science.

In 2017, Yang et al. reported the formation of Ag nanoparticles on CNFs using a metal salt precursor solution.[65] Electrospun PAN fibers were first carbonized at 1073 K for 2 h in Ar to form a CNF mat. The CNF mat was soaked in Ag acetate solution, dried, and then Joule heated to 1600 K up to 4 s. The resulting Ag/CNF hybrid contained 40 nm Ag nanoparticles on CNFs, which was used as an efficient 3D host for Li metal in Li metal batteries. The use of a similar approach was later extended to synthesize Pd nanoparticles supported on CNFs. CNFs were coated with PdCl$_2$ precursors and then heated to 2000 K, followed

by immediately cooling to room temperature. An important finding was that the size of Pd nanoparticles increased with the heating time. Their average size was 4.2 nm after 5 ms heating, 27.7 nm after 1 s heating, and more than 140 nm after 100 s cooling.[65] Qiao et al. further extended this method to Ni nanoparticles. Ni/rGO hybrids were constructed by anchoring 5 nm Ni nanoparticles onto a 3D-printed rGO framework via Joule heating. The sample was heated to 1900 K for 54 ms. When applied as cathodes in Li–CO$_2$ batteries, it showed a high areal capacity of 14.6 mAh cm^{-2}.[66] In 2019, this method was expanded to Ru nanoparticles. RuCl$_3$ aqueous solution was impregnated on two types of CNFs. One was carbonized under Ar at 1073 K, and the other activated CNFs were carbonized under CO$_2$ at 1073 K. As shown in Figure 4b, smaller Ru nanoparticles (4.1 nm) are more uniformly dispersed in activated CNFs after Joule heating, indicating that a suitable carbon substrate is essential in controlling the formation of metal nanoparticles. The Ru/C hybrid was used as catalyst in Li–CO$_2$ batteries.[67] The same approach of using activated CNFs was also applied to Pt, Ir, and Ni. The size of metal nanoparticles was tuned from >50 nm to <2 nm by optimizing the mass loading of metal precursors and defects in CNFs. The resulting metal/CNF hybrids were used as catalysts for CO oxidation.[67]

One recent adaptation of this method is using a more defective carbon substrate to increase the surface coverage of metal nanoparticles. As illustrated in Figure 4c, a CuCl$_2$-coated cellulose layer is loaded on carbon paper. During Joule heating, heat radiated from carbon paper carbonized the cellulose layer in 1.5 s. The partially carbonized cellulose provided many defects sites, leading to 85% Cu nanoparticle surface coverage. The Cu/C hybrid was used as catalyst for CO$_2$ reduction reaction. This method can also be applied to multielement alloy metal nanoparticles.[68] Another recent development is a continuous fly-through reactor designed for continuous catalyst synthesis. As shown in Figure 4d, metal salt precursors flow between two heated carbon sheets 1–3 mm apart under gravity and the carrier gas. The high temperature, up to 3200 K, enables the rapid decomposition of metal precursors into metal nanoparticles anchored on porous carbon black particles. The products can be collected at the bottom of the reactor. Using this new reactor, 4 nm Pt nanoparticles were anchored onto carbon black as an efficient electrocatalyst for the methanol oxidation reaction.[69]

Besides Joule heating, Smikhovskaia et al. reported an alternative ultrafast heating approach by laser-induced liquid-phase chemical deposition to obtain Ni nanoparticles.[70] NiCl$_2$ and a potassium–sodium tartrate solution were heated by laser irradiation (1.9–2.5 W), resulting in nanostructured Ni deposits. As mentioned earlier, microwave irradiation has also been used to synthesize various carbon-supported metal nanoparticles. Microwave-heated GO incorporated with Co, Cu, Fe, Ni nitrates, or PdCl$_2$ resulted in the formation of metal nanoparticles down to 3 nm in size.[25] Co, Ni, and Fe nanoparticles were anchored on carbon fibers using various MOF precursors.[26] Microwave irradiation was also used to heat carbon fiber cloth, graphite flasks, or carbonized wood to 1500 K, which were coated with Cu, Ni, Co, Zn, and Ag nitrates. The resulting metal/carbon hybrids were used as anodes in Li metal batteries.[27]

4.2. Carbon-Supported Metal Alloy/Metal Composite Nanoparticles

Bimetallic or multielemental alloy metal nanoparticles and composites often have very different catalytic activity than their monometallic counterparts. The ultrafast heating methods used to synthesize monometallic nanoparticles can also synthesize alloy nanoparticles by adding multiple metal precursors, as in several studies discussed in the previous subsection.[25,26,68] Furthermore, Chen et al. reported well-dispersed bimetallic Pd and Ni alloy nanoparticles supported on CNFs with good elemental mixing and uniform particle distribution. They achieved the fine tunings of the alloy nanoparticles' average size, chemical composition, and morphologies by controlling the chemical composition of metal precursors. The resulting Pd-Ni/CNF hybrids were used as catalysts for the hydrogen evolution reaction (HER) and hydrogen peroxide electrooxidation.[71] Jung et al. synthesized a large group of single, binary, ternary, and quaternary alloy particles of Pt, Pd, Au, and Ru using a similar method. The authors found that the quaternary alloy nanoparticles exhibited the best catalyst performance for the oxygen reduction reaction (ORR) and oxygen evolution reaction (OER) in Li–O$_2$ batteries.[72] Alternatively, Gong et al. reported the formation of metastable NiFe alloy heterostructure using microwave irradiation.[73] It was proposed that ultrafast heating could produce nanostructures beyond thermodynamic equilibrium limitations. The resulting NiFe particles contained amorphous and crystalline phases covered by a graphene shell, demonstrating the good catalytic performance of OER.

Ultrafast heating methods have also been used to synthesize transition metal carbides. Xie et al. incorporated 70–120 nm Si nanoparticles into electrospun PAN fibers. SiC/C necklace-like structures were formed after Joule heating at 2000 K for 40 s, which also improved the bond strength between C and homogenously dispersed SiC.[74] In 2021, Reynard et al. reported using flashlight heating to convert MnO$_3$/graphene mixture into Mo$_2$C as HER catalysts. The Mo$_2$C catalyst showed a Tafel slope of 63 mV dec^{-1} and a low overpotential of 160 mV at 10 mA cm^{-2} in 1 M H$_2$SO$_4$.[75]

4.3. Carbon-Supported HEA Nanoparticles

A unique class of metal alloy materials is HEAs, in which five or more metal elements are uniformly mixed with similar molar concentrations.[76] HEAs have attracted significant interest because of their unique properties, such as better mechanical strength and improved corrosion and oxidation resistance. However, it is challenging to synthesize them using conventional alloying methods due to the phase segregation of different elements. In 2018, Yao et al. reported a comprehensive study on using Joule heating as a general method to convert up to eight distinct elements (Pt, Pd, Ni, Co, Fe, Au, Cu, and Sn) with different atomic radii, redox potentials, preferred crystal structures, and melting temperatures into single-phase solid-solution HEA nanoparticles. CNFs loaded with different metal precursors were heated to 2000 K in less than 55 ms with a rapid heating rate of 10^5 K s^{-1}, followed by 10^5 K s^{-1} cooling. As illustrated in Figure 4e, a catalytically driven particle dispersion mechanism

was proposed to describe the formation of metal nanoparticles. Metal salt precursors first decompose into micrometer-sized liquid metal droplets at 2000 K ($MCl_xH_y \rightarrow M$ (liquid) + gases↑). These liquid metal droplets catalyze carbon metabolism reaction ($C + O^* \rightarrow CO\uparrow$) of surface-bound oxygen (O^*) residues on carbon fibers to create surface defects, leading to frequent metal droplet motion and split (fission), that is, over 10^6 times during the 55 ms heating period. The catalytic metabolism-induced metal particle fission/fusion is different from standard alloying methods. A liquid alloy is then transferred into a single-phase solid solution (with a size of around 10 nm) with a specific elemental composition under the cooling rate of $10^5 \, K \, s^{-1}$. In contrast, phase separation would occur when cooled slowly. Based on this mechanism, the authors showed that the density of surface-bound O, heating time, and cooling rate all could influence the size and composition of the resulting alloy particles. Quinary PtPdRhRuCe HEA particles were demonstrated as an efficient ammonia oxidation catalyst.[8] Alternatively, Qiao et al. reported the synthesis of HEA nanoparticles using microwave irradiation heating. Carbon substrates, such as rGO film, CNFs, or carbonized wood located with metal salt precursors, were sealed in an Ar-filled glass bottle. The temperature can reach 1850 K under 1200 W microwave irradiation in 10 s, resulting in the formation of 12 nm PtPdFeCoNi HEA nanoparticles.[77]

4.4. Carbon-Supported SACs

Since the demonstration of single Pt atom dopants in FeO_x in 2011,[78] SACs have attracted significant interest because of their high atom utilization efficiency, unique quantum size effects, and well-defined catalytic active sites. Some SACs contain catalytically active metal atoms atomically stabilized in electrical conductive carbon substrates and are potential electrocatalysts for energy storage and conversion.[79] Synthesis of such carbon-supported SACs usually involves high-temperature metal and carbon precursors treatments. However, metal agglomeration
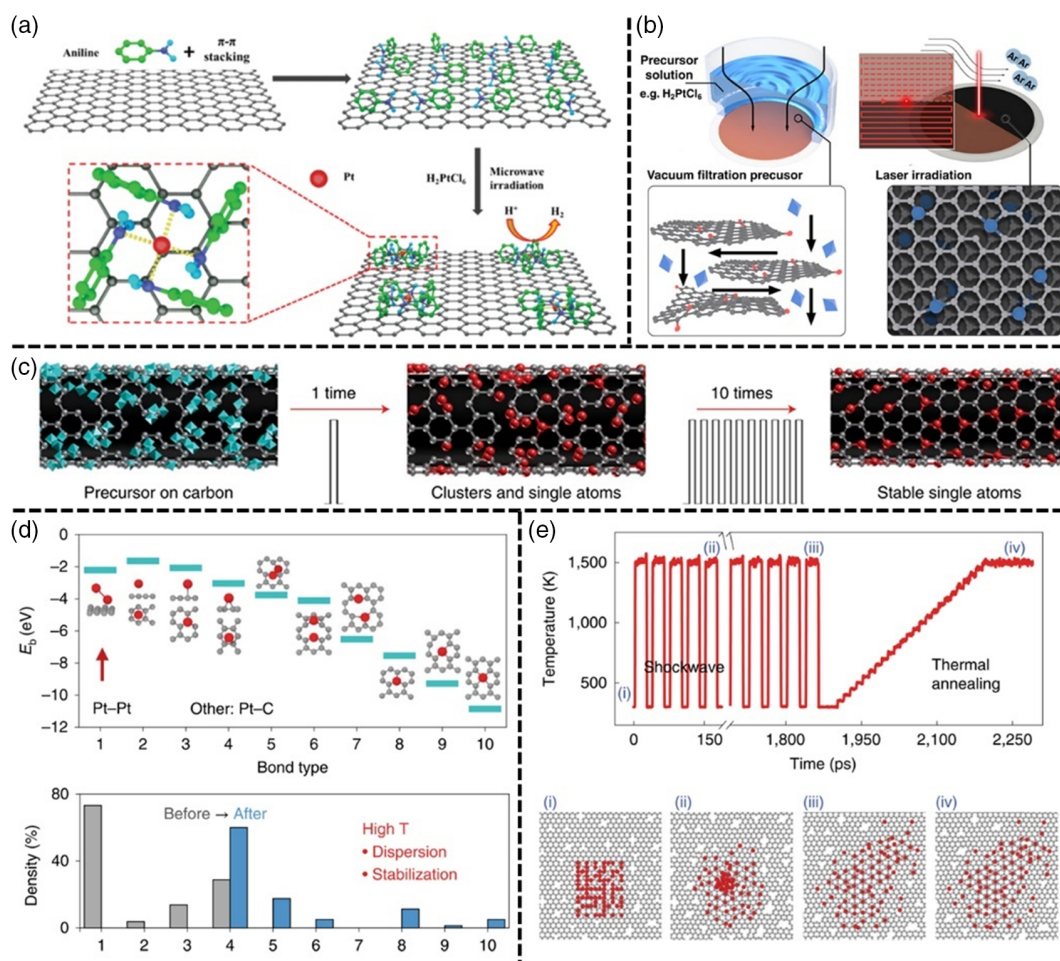

Figure 5. a) Schematic illustration of Pt SACs synthesis by microwave irradiation of graphene, aniline, and Pt precursors. Reproduced with permission.[81] Copyright 2019, Royal Society of Chemistry. b) Schematic illustration of laser irradiation of GO films loaded with Pt precursors to form Pt SACs. Reproduced with permission.[80b] Copyright 2021, Springer Nature. c) Schematic illustration of SAC synthesis by Joule heating. d) Bonding energy of Pt—Pt and Pt—C bonds (top) and the statistical distribution of different bonds before and after Joule heating (bottom). e) Molecular dynamic simulation on Pt single-atom dispersion (i to iii) and subsequent annealing at 1500 K (iv) on a defective graphene surface. Reproduced with permission.[82] Copyright 2019, Springer Nature.

often occurs during the high-temperature treatment, lowering the number of catalytically active sites and catalyst stability.[80] Ultrafast heating methods have been explored to synthesize carbon-supported SACs. The high temperature allows the decomposition of metal precursors, while the short heating time and fast cooling inhibit metal agglomeration.

In 2019, Ye et al. used microwave irradiation to synthesize Pt SACs supported on graphene for HER catalysis. As shown in **Figure 5**a, graphene substrate was first functionalized by aniline. H_2PtCl_6 was used as the Pt precursor. After microwave irradiation over 2 min, single Pt atoms were anchored on graphene via aniline. This catalyst with 0.44 wt% Pt demonstrated better activity and stability than 20 wt% Pt/C catalysts for HER in 0.5 M H_2SO_4 electrolyte.[81] Alternatively, Pt SACs were also synthesized by laser irradiation. As illustrated in Figure 5b, Pt precursors were adsorbed onto 1.5 µm-thick GO film by vacuum filtration. After freeze drying, the GO film was irradiated by a 1064 nm infrared laser or a 355 nm ultraviolet laser under 1000 mm s^{-1} scanning speed. The adsorbed laser energy was converted into local heat and raised the temperature, which reduced GO and decomposed metal precursors simultaneously. The resulting Pt/C hybrid contained 0.41 wt% single Pt atoms, which were used as an HER electrocatalyst.[80b]

Yao et al. reported a comprehensive study to demonstrate that Joule heating can be used to synthesize SACs. As illustrated in Figure 5c, a low concentration of Pt precursors (0.01 µmol cm^{-2} H_2PtCl_6) was first loaded on defect-activated CNFs. Then the Pt-loaded carbon film was heated to 1500 K for 55 ms and rapidly quenched to 400 K over 550 ms. Ten heating cycles were repeated over 6 s, resulting in stable 0.24 wt% Pt SACs. The catalysts showed excellent stability after heating at 1273 K for 1 h and can withstand thermal shock up to 2000 K. They also showed exceptional stability during CO oxidation and direct CH_4 conversion. Density functional theory (DFT) calculations and molecular dynamic simulation were used to understand why SACs were obtained compared with metal nanoparticles obtained in other Joule heating studies. Figure 5d shows that the bonding energy of Pt—C bonds is higher than the Pt—Pt bond. Several Pt—C bonds with Pt atoms coordinated by multiple carbon atoms (types 4–10) in a carbon frame are stronger than Pt linked with one carbon atom (types 1–3). Molecular dynamic simulation shows that Pt clusters disperse into individual atoms on a defective graphene surface with heating cycles at 1500 K. Figure 5e indicates that the dispersion becomes stable when annealed at 1500 K. The authors proposed that a higher temperature is critical to provide sufficient activation energy for atom diffusion and overcome the energy barrier for the formation of more stable Pt—C bonds. Further, the low metal loading and defective site density on carbon surfaces are crucial for forming SACs. In addition, semiconductive C_3N_4 and insulating TiO_2 can also be loaded on a carbon film to serve as substrates for SACs.[82]

Transition metal and N-codoped carbon-based SACs/carbon-supported N-coordinated transition metal SACs (metal–N–C) have shown outstanding activity in various reactions. N doping in carbon substrates is critical in stabilizing transition metal single atoms. However, excess N would lead to uncoordinated N species that are less stable and can affect electronic structures of catalytically active metal sites, resulting in reduced stability and activity. Xi et al. used Joule heating to minimize

uncoordinated N in a carbon-supported Ni SAC for CO_2 reduction reaction. 1,10-phenanthroline-Ni acetate adsorbed on carbon black was heated to 1573 K for 0.5 s. Uncoordinated N species were removed at high temperatures, and 80% N were coordinated with transition metal atoms. The catalyst showed a CO selectivity over 92% under a wide potential window.[83] This method can also be extended to other transition metals, such as Fe, Co, Cu, and Zn. Lu et al. carried out Joule heating of Co ion-loaded porous CNFs at a relatively low temperature of 1023 K. The resulting Co/carbon hybrid contained 5–7 nm Co nanoparticles and Co–N–C, which were used as a bifunctional catalyst for ORR and OER in Zn–air batteries.[84] In a recent study, $CoCl_2$ was loaded on NH_3-treated GO. Upon Joule heating under NH_3 atmosphere, Co–N–C catalysts were obtained with 0.81 wt% Co loading.[85]

5. Summary and Future Perspectives

Thermal treatment plays a crucial role in carbon material synthesis. Recent progress in ultrafast heating methods, including Joule heating, laser, light, or microwave irradiations, has led to novel carbon materials and carbon/metal hybrid structures. Some of these materials have shown excellent application potentials, such as turbostratic graphene, environmentally responsive rGO/GO hybrids, welded high-electrical-conductivity rGO films and CNT architectures, homogenous metal alloy nanoparticles, HEA nanoparticles, and stable SACs. The ultrafast heating methods can achieve faster heating (up to 10^5 K s^{-1}) to reach higher temperatures (e.g., 3000 K) and quicker heating and cooling rates (up to 10^5 K s^{-1}) than those of traditional heating methods. Their benefits for material synthesis may include prompt and often complete decomposition of carbon and metal precursors; efficient nanoscale welding of various carbon materials, efficient doping of heteroatoms into carbon materials, fast graphitization of carbon precursors, significantly limited agglomeration of metal specie, uniform dispersion of small metal nanoparticles or stabilized single-metal atoms, the formation of single-phase solid-solution alloy particles from elements with different properties, targeted heating treatment at specific locations based on local electrical resistance or focused irradiation, and a significant reduction in the energy consumption due to shorter heat treatment time.

Though impressive progress that has been achieved in the last few years, there are still significant knowledge gaps and technical challenges in implementing ultrafast heating methods for the scalable production of carbon and carbon/metal hybrids. We propose the following areas as priorities in the upcoming research studies.

First, understanding the carbonization and graphitization mechanisms under ultrafast heating conditions remains vague. Most material synthesis studies focus on equilibrium reaction conditions with slow temperature changes or at constant temperatures. Although we expect reaction kinetics and mass transport to play more critical roles when heating and cooling occur in milliseconds or seconds, many issues are unclear. For example, does the removal of noncarbon species from carbon precursors depend only on temperature? Will mass transfer limit the removal of noncarbon species? How will the gas environment

affect carbonization and potentially induce doping of heteroatoms? How will the long-range order of carbon layers change under fast varying temperatures? What is the growth rate of graphitic carbon layers? What is the timescale that may allow the alignment of graphitic carbon layers? The short time scale and high temperature make mechanistic studies very challenging. Combining in situ ultrafast spectroscopies and molecular dynamic simulations may help answer some of these questions. Obtaining an improved mechanistic understanding will be critical in better controlling ultrafast heating methods to get materials with desirable characteristics. Future studies in this field should focus on two aspects: first, fine tuning ultrafast heating parameters to better control carbon structures during carbonization and graphitization and second, finding specific conditions required for the removal, retainment, and addition of different heteroatom dopants and phase transitions within carbon and carbon-based hybrid materials to enable the design of advanced functional materials for specific applications.

Second, the temperature uniformity at a large scale is another limiting factor. In most studies reported, temperature uniformity is not a problem for carbon substrates with a lateral dimension at centimeters and thickness at micrometers. However, achieving uniform temperature will likely become a critical challenge when we try to scale up ultrafast heating methods. For example, Joule heating depends on the electrical resistance of carbon substrates. Defects in carbon framework or junctions between adjoining carbon nanostructures have higher electrical resistance than intact graphitic planes or surfaces. These places would become high-temperature spots during Joule heating. We need to understand whether the thermal conductivity of different carbon substrates is sufficient to allow efficient heat conduction/dissipation from high-temperature zones to enable temperature uniformity over larger spatial dimensions. Achieving temperature uniformity will become more complicated for heating methods based on laser, light, or microwave irradiation. The penetration depth of light sources or microwaves, absorptivity, and photothermal effects at different wavelengths in different carbon substrates will influence temperature distribution. Understanding their relationships will be essential for better control over these heating methods.

Next, creating uniform surface-bound oxygen (O*) residues is still a challenging task. The recently proposed catalytically driven particle dispersion mechanism[8] suggests that O* and resulting defect sites play critical roles in achieving the atomic dispersion of metal atoms. However, few studies have examined how to uniformly introduce surface-bound oxygen (O*) or defect sites onto different carbon substrates without significantly affecting/disturbing their electrical conductivity and other photothermal properties. The efficiency and consistency of existing methods, such as CO_2 oxidative activation, rely on reaction conditions and carbon substrate properties. It isn't easy to regulate them to achieve nanoscale uniformity. Innovations in carbon substrates to create uniform surface-bound oxygen (O*) residues and novel metal precursors with well-defined atomic structures may help to improve the synthesis control of carbon/metal hybrid structures using ultrafast heating methods.

Furthermore, energy consumption at a larger scale is also critical. Compared with conventional heating methods, the significantly lower energy consumption of the ultrafast heating processes reported in recent studies is limited to heating materials at a centimeter scale or smaller. The heating zone in conventional furnaces, spray pyrolysis, or solvothermal reactors are one or two orders larger. To realize large-scale material production by ultrafast heating methods will likely require a much larger heating area, which may lead to significant heat loss. Systematic heat and mass transfer analysis and instrument innovation will be needed to understand the energy consumption in these conditions and achieve minimized energy consumption for practical applications.

In addition, the scalability and technical readiness of these fast-heating techniques for practical applications should be evaluated. Several studies have proposed scalable ultrafast heating methods for material synthesis.[7,9,62,69] Their scalability is still limited to a lab-scale demonstration. Comprehensive chemical process studies are needed to understand their production yield, material property consistency, instrument costs, and operating costs. These studies will be essential if they want to compete with conventional material synthesis methods.

Finally, a wide range of energy storage, sensors, and electrocatalysis applications has been explored for novel materials synthesized by ultrafast heating methods. However, more efforts are required to carefully examine the technical readiness level of these materials and identify applications that could benefit the most to carry out future studies.

Ultrafast heating methods have opened excellent opportunities for material syntheses and have shown promise in various applications. This exciting area calls for more research to narrow gaps in fundamental understandings and resolve technical challenges. We hope that future research can resolve these issues and develop them into mainstream material synthesis methods for producing critical materials that can address current challenges in different fields.

Acknowledgements

Conflict of Interest

The authors declare no conflict of interest.

Keywords

[1] M. Inagaki, F. Y. Kang, *Materials Science and Engineering Of Carbon: Fundamentals*, Elsevier Inc., Oxford, UK **2014**.

[2] H. W. Kroto, J. R. Heath, S. C. O'Brien, R. F. Curl, R. E. Smalley, *Nature* **1985**, *318*, 162.

[3] S. Iijima, *Nature* **1991**, *354*, 56.

[4] P. J. Harris, *Carbon* **2017**, *122*, 504.

[5] Y. Yao, K. K. Fu, S. Zhu, J. Dai, Y. Wang, G. Pastel, Y. Chen, T. Li, C. Wang, T. Li, *Nano Lett.* **2016**, *16*, 7282.

[6] Y. Yao, F. Jiang, C. Yang, K. K. Fu, J. Hayden, C.-F. Lin, H. Xie, M. Jiao, C. Yang, Y. Wang, *ACS Nano* **2018**, *12*, 5266.

[7] Y. Liu, P. Li, F. Wang, W. Fang, Z. Xu, W. Gao, C. Gao, *Carbon* **2019**, *155*, 462.

[8] Y. Yao, Z. Huang, P. Xie, S. D. Lacey, R. J. Jacob, H. Xie, F. Chen, A. Nie, T. Pu, M. Rehwoldt, *Science* **2018**, *359*, 1489.

[9] D. X. Luong, K. V. Bets, W. A. Algozeeb, M. G. Stanford, C. Kittrell, W. Chen, R. V. Salvatierra, M. Ren, E. A. McHugh, P. A. Advincula, *Nature* **2020**, *577*, 647.

[10] M. G. Stanford, K. V. Bets, D. X. Luong, P. A. Advincula, W. Chen, J. T. Li, Z. Wang, E. A. McHugh, W. A. Algozeeb, B. I. Yakobson, *ACS Nano* **2020**, *14*, 13691.

[11] a) W. A. Algozeeb, P. E. Savas, D. X. Luong, W. Chen, C. Kittrell, M. Bhat, R. Shahsavari, J. M. Tour, *ACS Nano* **2020**, *14*, 15595; b) K. M. Wyss, J. L. Beckham, W. Chen, D. X. Luong, P. Hundi, S. Raghuraman, R. Shahsavari, J. M. Tour, *Carbon* **2021**, *174*, 430; c) P. A. Advincula, D. X. Luong, W. Chen, S. Raghuraman, R. Shahsavari, J. M. Tour, *Carbon* **2021**, *178*, 649; d) N. H. Barbhuiya, A. Kumar, A. Singh, M. K. Chandel, C. J. Arnusch, J. M. Tour, S. P. Singh, *ACS Nano* **2021**, *15*, 15461.

[12] W. Chen, C. Ge, J. T. Li, J. L. Beckham, Z. Yuan, K. M. Wyss, P. A. Advincula, L. Eddy, C. Kittrell, J. A. N. Chen, *ACS Nano* **2022**, *16*, 6646.

[13] J. L. Beckham, K. M. Wyss, Y. Xie, E. A. McHugh, J. T. Li, P. A. Advincula, W. Chen, J. Lin, J. M. Tour, *Adv. Mater.* **2022**, *34*, 2106506.

[14] D. X. Luong, A. K. Subramanian, G. A. L. Silva, J. Yoon, S. Cofer, K. Yang, P. S. Owuor, T. Wang, Z. Wang, J. Lou, P. M. Ajayan, J. M. Tour, *Adv. Mater.* **2018**, *30*, 1707416.

[15] B. Yilbas, *Laser Heating Applications: Analytical Modelling*, Elsevier, Amsterdam **2012**.

[16] M. F. El-Kady, V. Strong, S. Dubin, R. B. Kaner, *Science* **2012**, *335*, 1326.

[17] J. Lin, Z. Peng, Y. Liu, F. Ruiz-Zepeda, R. Ye, E. L. G. Samuel, M. J. Yacaman, B. I. Yakobson, J. M. Tour, *Nat. Commun.* **2014**, *5*, 5714.

[18] J. L. Beckham, J. T. Li, M. G. Stanford, W. Y. Chen, E. A. McHugh, P. A. Advincula, K. M. Wyss, Y. E. Chyan, W. L. Boldman, P. D. Rack, J. M. Tour, *ACS Nano* **2021**, *15*, 8976.

[19] R. Ye, D. K. James, J. M. Tour, *Adv. Mater.* **2019**, *31*, 1803621.

[20] L. J. Wang, M. F. El-Kady, S. Dubin, J. Y. Hwang, Y. Shao, K. Marsh, B. McVerry, M. D. Kowal, M. F. Mousavi, R. B. Kaner, *Adv. Energy Mater.* **2015**, *5*, 1500786.

[21] H. Zhang, D. Yang, T. Ma, H. Lin, B. Jia, *Small Methods* **2021**, *5*, 2100225.

[22] R. B. Ambade, H. Lee, K. H. Lee, H. Lee, G. K. Veerasubramani, Y.-B. Kim, T. H. Han, *Chem. Eng. J.* **2022**, *436*, 135041.

[23] a) P. C. Sherrell, J. Chen, J. M. Razal, I. P. Nevirkovets, C. Crean, G. G. Wallace, A. I. Minett, *Energy Environ. Sci.* **2010**, *3*, 1979; b) M. Tsuji, M. Hashimoto, Y. Nishizawa, M. Kubokawa, T. Tsuji, *Eur. J. Chem.* **2005**, *11*, 440.

[24] A. Metaxas, *Power Eng. J.* **1991**, *5*, 237.

[25] X. Chen, X. Bo, W. Ren, S. Chen, C. Zhao, *Mater. Chem. Front.* **2019**, *3*, 1433.

[26] H. Huang, S. Zhou, C. Yu, H. Huang, J. Zhao, L. Dai, J. Qiu, *Energy Environ. Sci.* **2020**, *13*, 545.

[27] G. Zhong, S. Xu, Q. Dong, X. Wang, L. Hu, *Adv. Funct. Mater.* **2021**, *31*, 2010968.

[28] L. Lin, H. Peng, Z. Liu, *Nat. Mater.* **2019**, *18*, 520.

[29] a) S. Lee, M. F. Toney, W. Ko, J. C. Randel, H. J. Jung, K. Munakata, J. Lu, T. H. Geballe, M. R. Beasley, R. Sinclair, *ACS Nano* **2010**, *4*, 7524; b) M. G. Lemaitre, S. Tongay, X. Wang, D. K. Venkatachalam, S. Fridmann, B. P. Gila, A. F. Hebard, F. Ren, R. G. Elliman, B. R. Appleton, *Appl. Phys. Lett.* **2012**, *100*, 193105; c) I. Choi, H. Y. Jeong, H. Shin, G. Kang, M. Byun, H. Kim, A. M. Chitu, J. S. Im, R. S. Ruoff, S.-Y. Choi, *Nat. Commun.* **2016**, *7*, 1; d) T. Hu, H. Bao, S. Liu, X. Liu, D. Ma, F. Ma, K. Xu, *Carbon* **2017**, *120*, 219.

[30] a) Y. Li, D. X. Luong, J. Zhang, Y. R. Tarkunde, C. Kittrell, F. Sargunaraj, Y. Ji, C. J. Arnusch, J. M. Tour, *Adv. Mater.* **2017**, *29*, 1700496; b) L. X. Duy, Z. Peng, Y. Li, J. Zhang, Y. Ji, J. M. Tour, *Carbon* **2018**, *126*, 472.

[31] a) A. Ferrari, *Solid State Commun.* **2007**, *143*, 47; b) A. C. Ferrari, D. M. Basko, *Nat. Nanotechnol.* **2013**, *8*, 235.

[32] T. H. Im, D. Y. Park, H. K. Lee, J. H. Park, C. K. Jeong, D. J. Joe, K. J. Lee, *Part. Part. Syst. Charact.* **2017**, *34*, 1600429.

[33] S. Pei, H.-M. J. C. Cheng, *Carbon* **2012**, *50*, 3210.

[34] S.-H. Park, H.-S. Kim, *Nanotechnology* **2015**, *26*, 205601.

[35] Y. Chen, K. Fu, S. Zhu, W. Luo, Y. Wang, Y. Li, E. Hitz, Y. Yao, J. Dai, J. Wan, *Nano Lett.* **2016**, *16*, 3616.

[36] Y. Liu, C. Liang, A. Wei, Y. Jiang, Q. Tian, Y. Wu, Z. Xu, Y. Li, F. Guo, Q. Yang, *Mater. Today Nano* **2018**, *3*, 1.

[37] S. H. Noh, W. Eom, W. J. Lee, H. Park, S. B. Ambade, S. O. Kim, T. H. Han, *Carbon* **2019**, *142*, 230.

[38] H. B. Lee, S. H. Noh, T. H. Han, *Chem. Eng. J.* **2021**, *414*, 128803.

[39] S. I. Wong, H. Lin, Y. Yang, J. Sunarso, B. T. Wong, B. Jia, *J. Power Sources* **2020**, *478*, 228732.

[40] D. Chakravarty, C. S. Tiwary, C. F. Woellner, S. Radhakrishnan, S. Vinod, S. Ozden, P. A. da Silva Autreto, S. Bhowmick, S. Asif, S. A. Mani, *Adv. Mater.* **2016**, *28*, 8959.

[41] S. Yoo, S. Y. Jeong, J.-W. Lee, J. H. Park, D.-W. Kim, H. J. Jeong, J. T. Han, G.-W. Lee, S. Y. Jeong, *Carbon* **2019**, *144*, 675.

[42] H. Cheng, J. Liu, Y. Zhao, C. Hu, Z. Zhang, N. Chen, L. Jiang, L. Qu, *Angew. Chem. Int. Ed* **2013**, *52*, 10482.

[43] D. D. Han, Y. L. Zhang, H. B. Jiang, H. Xia, J. Feng, Q. D. Chen, H. L. Xu, H. B. Sun, *Adv. Mater.* **2015**, *27*, 332.

[44] a) Y. He, Y.-Q. Liu, J.-N. Ma, D.-D. Han, J.-W. Mao, C.-H. Han, Y.-L. Zhang, *IEEE Sens. J.* **2017**, *17*, 5285; b) Y.-Q. Liu, J.-N. Ma, Y. Liu, D.-D. Han, H.-B. Jiang, J.-W. Mao, C.-H. Han, Z.-Z. Jiao, Y.-L. Zhang, *Opt. Mater. Express* **2017**, *7*, 2617.

[45] I. H. Kim, T. H. Im, H. E. Lee, J. S. Jang, H. S. Wang, G. Y. Lee, I. D. Kim, K. J. Lee, S. O. Kim, *Small* **2019**, *15*, 1901529.

[46] Y. Jeon, X. Han, K. Fu, J. Dai, J. H. Kim, L. Hu, T. Song, U. Paik, *J. Mater. Chem. A* **2016**, *4*, 18306.

[47] F. Zhang, Y. Yao, J. Wan, D. Henderson, X. Zhang, L. Hu, *ACS Appl. Mater. Interfaces* **2017**, *9*, 391.

[48] Y. Zhen, Y. Chen, F. Li, Z. Guo, Z. Hong, M.-M. Titirici, *Proc. Natl. Acad. Sci.* **2021**, *118*, 2111119118.

[49] M. Terrones, H. Terrones, F. Banhart, J.-C. Charlier, P. Ajayan, *Science* **2000**, *288*, 1226.

[50] T. Yuzvinsky, W. Mickelson, S. Aloni, G. Begtrup, A. Kis, A. Zettl, *Nano Lett.* **2006**, *6*, 2718.

[51] C. Jin, K. Suenaga, S. Iijima, *Nat. Nanotechnol.* **2008**, *3*, 17.

[52] L. Zhao, Y. Cheng, Q. Zhang, M.-S. Wang, *Mater. Horiz.* **2019**, *6*, 72.

[53] X. Gong, H. Zhang, Z. Sun, X. Zhang, J. Xu, F. Chu, L. Sun, S. Ramakrishna, *Nanoscale* **2020**, *12*, 13095.

[54] a) C. Lim, J. H. Jang, D. J. Bae, G. H. Han, S. Lee, I.-S. Yeo, Y. H. Lee, *Appl. Phys. Lett.* **2009**, *95*, 264103; b) A. Maiti, A. Ricca, *Chem. Phys. Lett.* **2004**, *395*, 7.

[55] J. Zou, X. Zhang, C. Xu, J. Zhao, Y. T. Zhu, Q. Li, *Carbon* **2017**, *121*, 242.

[56] Y.-T. Liu, T.-T. Yao, W.-S. Zhang, G.-P. Wu, *Mater. Lett.* **2019**, *236*, 244.

[57] W. Bao, A. D. Pickel, Q. Zhang, Y. Chen, Y. Yao, J. Wan, K. Fu, Y. Wang, J. Dai, H. Zhu, D. Drew, M. Fuhrer, C. Dames, L. Hu, *Adv. Mater.* **2016**, *28*, 4684.

[58] P. Nautiyal, L. Embrey, B. Boesl, A. Agarwal, *Carbon* **2017**, *122*, 298.

[59] K. Wang, J. Pang, L. Li, S. Zhou, Y. Li, T. Zhang, *Front. Chem. Sci. Eng.* **2018**, *12*, 376.

[60] S. Liu, P. Wang, C. Liu, Y. Deng, S. Dou, Y. Liu, J. Xu, Y. Wang, W. Liu, W. Hu, Y. Huang, Y. Chen, *Small* **2020**, *16*, 2002856.

[61] C. Chen, Y. Chen, S. Zhu, J. Dai, G. Pastel, Y. Yao, D. Liu, Y. Wang, J. Wan, T. Li, *Research* **2018**, *2018*.

[62] Y. Shang, B. Shi, S. M. Doshi, T. Chu, G. Qiu, A. Du, Y. Zhao, F. Xu, E. T. Thostenson, K. K. Fu, *ACS Appl. Mater. Interfaces* **2020**, *12*, 37722.

[63] Y. Chen, Y. Li, Y. Wang, K. Fu, V. A. Danner, J. Dai, S. D. Lacey, Y. Yao, L. Hu, *Nano Lett.* **2016**, *16*, 5553.

[64] Y. Li, Y. Chen, A. Nie, A. Lu, R. J. Jacob, T. Gao, J. Song, J. Dai, J. Wan, G. Pastel, *Adv. Energy Mater.* **2017**, *7*, 1601783.

[65] C. Yang, Y. Yao, S. He, H. Xie, E. Hitz, L. Hu, *Adv. Mater.* **2017**, *29*, 1702714.

[66] Y. Qiao, Y. Liu, C. Chen, H. Xie, Y. Yao, S. He, W. Ping, B. Liu, L. Hu, *Adv. Funct. Mater.* **2018**, *28*, 1805899.

[67] Y. Qiao, S. Xu, Y. Liu, J. Dai, H. Xie, Y. Yao, X. Mu, C. Chen, D. J. Kline, E. M. Hitz, B. Liu, J. Song, P. He, M. R. Zachariah, L. Hu, *Energy Environ. Sci.* **2019**, *12*, 1100.

[68] J.-Y. Song, C. Kim, M. Kim, K. M. Cho, I. Gereige, W.-B. Jung, H. Jeong, H.-T. Jung, *Sci. Adv.* **2021**, *7*, eabk2984.

[69] Y. Qiao, C. Chen, Y. Liu, Y. Liu, Q. Dong, Y. Yao, X. Wang, Y. Shao, C. Wang, L. Hu, *Nano Lett.* **2021**, *21*, 4517.

[70] A. Smikhovskaia, S. Kochemirovskaya, M. Novomlinskii, D. Lebedev, V. Kochemirovsky, S. Ermakov, L. Menchikov, *Russ. Chem. Bull.* **2019**, *68*, 2020.

[71] F. Chen, Y. Yao, A. Nie, S. Xu, J. Dai, E. Hitz, Y. Li, A. Lu, Z. Huang, T. Li, *Adv. Energy Mater.* **2018**, *8*, 1800466.

[72] W.-B. Jung, H. Park, J.-S. Jang, D. Y. Kim, D. W. Kim, E. Lim, J. Y. Kim, S. Choi, J. Suk, Y. Kang, I.-D. Kim, J. Kim, M. Wu, H.-T. Jung, *ACS Nano* **2021**, *15*, 4235.

[73] Z. Gong, R. Liu, H. Gong, G. Ye, J. Liu, J. Dong, J. Liao, M. Yan, J. Liu, K. Huang, L. Xing, J. Liang, Y. He, H. Fei, *ACS Catal.* **2021**, *11*, 12284.

[74] H. Xie, K. Fu, C. Yang, Y. Yao, J. Rao, Y. Zhou, B. Liu, D. Kirsch, L. Hu, *Small Methods* **2018**, *2*, 1700371.

[75] D. Reynard, B. Nagar, H. Girault, *ACS Catal.* **2021**, *11*, 5865.

[76] J. W. Yeh, S. K. Chen, S. J. Lin, J. Y. Gan, T. S. Chin, T. T. Shun, C. H. Tsau, S. Y. Chang, *Adv. Eng. Mater.* **2004**, *6*, 299.

[77] H. Qiao, M. T. Saray, X. Wang, S. Xu, G. Chen, Z. Huang, C. Chen, G. Zhong, Q. Dong, M. Hong, H. Xie, R. Shahbazian-Yassar, L. Hu, *ACS Nano* **2021**, *15*, 14928.

[78] B. Qiao, A. Wang, X. Yang, L. F. Allard, Z. Jiang, Y. Cui, J. Liu, J. Li, T. Zhang, *Nat. Chem.* **2011**, *3*, 634.

[79] Y. Yang, Y. Yang, Z. Pei, K.-H. Wu, C. Tan, H. Wang, L. Wei, A. Mahmood, C. Yan, J. Dong, S. Zhao, Y. Chen, *Matter* **2020**, *3*, 1442.

[80] a) Z. Miao, S. Li, C. Priest, T. Wang, G. Wu, Q. Li, *Adv. Mater.* **2022**, 2200595; b) Y. Peng, J. Cao, Y. Sha, W. Yang, L. Li, Z. Liu, *Light Sci. Appl.* **2021**, *10*, 168.

[81] S. Ye, F. Luo, Q. Zhang, P. Zhang, T. Xu, Q. Wang, D. He, L. Guo, Y. Zhang, C. He, *Energy Environ. Sci.* **2019**, *12*, 1000.

[82] Y. Yao, Z. Huang, P. Xie, L. Wu, L. Ma, T. Li, Z. Pang, M. Jiao, Z. Liang, J. Gao, Y. He, D. J. Kline, M. R. Zachariah, C. Wang, J. Lu, T. Wu, T. Li, C. Wang, R. Shahbazian-Yassar, L. Hu, *Nat. Nanotechnol.* **2019**, *14*, 851.

[83] D. Xi, J. Li, J. Low, K. Mao, R. Long, J. Li, Z. Dai, T. Shao, Y. Zhong, Y. Li, *Adv. Mater.* **2021**, 2104090.

[84] Q. Lu, H. Wu, X. Zheng, Y. Chen, A. L. Rogach, X. Han, Y. Deng, W. Hu, *Adv. Sci.* **2021**, *8*, 2101438.

[85] L. Xing, R. Liu, Z. Gong, J. Liu, J. Liu, H. Gong, K. Huang, H. Fei, *Nano Res.* **2022**, *15*, 3913.

[86] Y. Chen, Y. Li, Y. Wang, K. Fu, V. A. Danner, J. Dai, S. D. Lacey, Y. Yao, L. Hu, *Nano Lett.* **2016**, *16*, 5553.

Leo Lai received his B.Eng. (Hons) from the University of Sydney in 2021. He is currently a Ph.D. student under the supervision of Professor Yuan Chen at the University of Sydney. His research interests focus on the design of advanced electrocatalysts for renewable energy conversion and storage.

Yuan Chen received a bachelor's degree from Tsinghua University and a Ph.D. from Yale University. He is a professor at The University of Sydney. His research focuses on carbon materials and their sustainable energy and environmental applications, including batteries, supercapacitors, electrocatalysts, membranes, and antibacterial coatings. He is a fellow of the Royal Society of Chemistry and the Institution of Chemical Engineers. He is currently serving as an editor for Carbon and Journal of Alloys and Compounds.